Fokker Planck kinetic modeling of suprathermal alpha-particles in a fusion plasma

Benjamin-Edouard Peigney, Olivier Larroche, Vladimir Tikhonchuk

Fokker Planck kinetic modeling of suprathermal α-particles in a fusion plasma

B. E. Peigney[a,*], O. Larroche[a], V. Tikhonchuk[b]

[a] *CEA/DIF, 91297 Arpajon Cedex, France*
[b] *University Bordeaux – CNRS – CEA, CELIA 33405 Talence Cedex, France*

Abstract

We present an ion kinetic model describing the transport of suprathermal α-particles in inertial fusion targets. The analysis of the underlying physical model enables us to develop efficient numerical methods to simulate the creation, transport and collisional relaxation of fusion reaction products (α-particles) at a kinetic level. The model assumes spherical symmetry in configuration space and axial symmetry in velocity space around the mean flow velocity. A two-energy-scale approach leads to a self-consistent modeling of the coupling between suprathermal α-particles and the thermal bulk of the imploding plasma. This method provides an accurate numerical treatment of energy deposition and transport processes involving suprathermal particles. The numerical tools presented here are then validated against known analytical results. This enables us to investigate the potential role of ion kinetic effects on the physics of ignition and thermonuclear burn in inertial confinement fusion schemes.

Keywords: Fokker-Planck equation, fusion reactions, kinetic effects, inertial confinement fusion plasma, suprathermal particles, multi-scale coupling, explicit schemes

1. Purpose of the study

Inertial confinement fusion (ICF) is a process of energy production obtained from the nuclear fusion reaction between deuterium (D) and tritium (T) ions. It is a promising and abundant energy source for future power plants. The fusion reactions $D + T \rightarrow \alpha + n + 17.56\,\mathrm{MeV}$ take place in a hot and dense plasma compressed and heated by intense laser radiation. The thermonuclear burn of the deuterium-tritium (DT) fuel is supported by energetic α-particles, which are created by fusion reactions at the energy 3.52 MeV. Those suprathermal particles subsequently transfer their energy to the dense fuel through Coulomb collisions.

In ICF [1, 2], a spherical DT shell is compressed to densities of the order of a few hundred $\mathrm{g.cm^{-3}}$ by the so-called ablation pressure, which builds up as the low-Z pusher surrounding the fuel is ablated by the incoming energy flux (Laser or X flux). Fusion reactions start in a central zone characterized by a density $\rho \sim 50\,\mathrm{g.cm^{-3}}$ and a high temperature $T \approx 7 - 10\,\mathrm{keV}$. The density of the central hot spot is such that the mean free path λ_α of fast α-particles is roughly equal to the hot spot radius R [3]. This allows the self-heating of the hot spot fuel which serves as a spark that subsequently triggers the propagation of a burn front through the surrounding colder and denser shell.

The design of ICF targets and the interpretation of ICF experiments rely on numerical simulations based on hydrodynamic Lagrangian codes where kinetic effects are only considered as corrections included in the transport coefficients [1, 2]. The fluid description is relevant if the mean free path of plasma particles, namely electrons and ions, is smaller than the characteristic length scale. Although this condition is reasonably fulfilled during the implosion stage, it does not apply to fast fusion products. Thus, an accurate kinetic modeling of energetic α-particles is required.

In this work we propose an ion-kinetic description of suprathermal fusion products, treated self-consistently with the ion-kinetic modeling of the thermal imploding plasma. The difficulty lies in the coupling of ion populations characterized by two different energy scales:

- Thermal D,T ions, which form the bulk of the imploding plasma and whose kinetic energy is in the keV range.

*benjamin.peigney@mines-paris.org

- Suprathermal α-particles, created at 3.52 MeV by fusion reactions.

Such a strong disparity in energy scales makes it difficult to build viable kinetic models of fusion reactions.

Existing ion kinetic codes can describe the implosion of DT targets in sub-ignition conditions [4, 5, 6], but the energy release from fusion reactions is not accounted for in a self-consistent manner. Several simplified methods compatible with hydrodynamic codes have been developed. Haldy and Ligou [7] apply the moment method to model ion energy deposition in a hot and dense homogeneous plasma, but only a stationary case has been considered. A variety of methods based on diffusion models applied to charged-particle transport problems have also been designed. Those methods are of considerable interest, since results on energy deposition profiles can be obtained with a low computational effort. Nevertheless, diffusion methods rely on the assumption that the fast particle mean free path is smaller than the characteristic scale length of the energy deposition zone. This hypothesis does not hold for a typical ICF target near ignition and during combustion. Corman et al [8] derive a multi-group diffusion model from the Fokker-Planck equation to describe fast ion transport in a fusion plasma. However, they introduce heuristically a flux limiter in order to prevent unphysical behavior when the particle flux approaches the free-streaming limit. Pomraning [9] develops a more sophisticated flux limiter scheme based on the Chapman-Enskog expansion. Nonetheless, the flux limited diffusion artificially smoothes energy deposition profiles, especially in situations where ion sources are localized [10]. This may lead to significant errors in the calculation of ignition thresholds and energy gains. Such diffusion models are employed in all major present-day fluid codes because of their compatibility with the underlying hydrodynamic module.

Several exact methods can be employed to solve the Fokker-Planck equation in a general way, but they are too much time consuming. Monte Carlo algorithms are applied to model charged particle transport in Refs. [11, 12]. In such an approach, distribution functions are represented by a sum of Dirac measures. Monte Carlo particles are characterized by their numerical weight, their position and their velocity. Those quantities evolve in time according to the Vlasov-Fokker-Planck equation while the tracking of Monte Carlo particles is performed through the spatial mesh. The accuracy of Monte Carlo methods is proportional to $N^{-1/2}$, N being the number of Monte Carlo particles, so that $N \gg 1$ and variance reduction techniques are usually employed to reduce numerical noise. Even if those methods are interesting in 2D/3D geometries, they are less efficient than deterministic approaches for 1D problems. In particular, a significant deficiency of Monte Carlo methods for the investigation of kinetic effects is that the tails of the distribution functions are not described accurately. The self-consistent modeling of energy and momentum transport of suprathermal α-particles, as well their interaction with the electric field requires a complete ion-kinetic description. Moreover, the coupling between suprathermal particles and the thermal bulk is usually treated in a rough manner, by removing the suprathermal particles that are slowed down below a given energy threshold and injecting the removed particles in the thermal bulk. Therefore, the thermalization process is not described with sufficient precision.

S_n methods are also used to solve the Fokker-Planck equation deterministically. They are based on the determination of the angular flux of suprathermal particles at a set of discrete directions, each one associated with a quadrature weight [13, 14]. Although they are more accurate than diffusion methods and can be extended to highly anisotropic particle distribution functions, the weakly collisional limit is not described accurately and the thermalization process is treated approximately with the same strategy as in Monte Carlo methods. S_n methods are usually used to simulate neutron transport and require high computational efforts. For the application of S_n methods to suprathermal α-particles transport, we refer to Ref. [10].

In this work we develop a full and self-consistent ion kinetic modeling of suprathermal fusion products in the thermal imploding plasma. We extend the existing code Fpion [4, 5, 6] so as to treat α-particles, for which *two scales of energy* are considered, namely a suprathermal and a thermal one. Since the developments made to reach this goal have been substantial, an entirely new kinetic code called Fuse for Fpion *Upgrade with two Scales of Energy* has been designed. This code is able to investigate kinetic effects related to fusion reaction products on the ignition of the hot spot and on the subsequent propagation of the thermonuclear burn wave through the dense fuel. We present here the numerical methods specially developed for the kinetic modeling of α-particles and their validation in several representative tests. Simulations are peformed for a typical ICF DT target. Comparisons between the fluid code FCI1 and the kinetic code Fuse are presented during the implosion and the propagation of the combustion flame through the dense fuel shell.

The paper is organized as follows: firstly, we present in Section 2 the Vlasov-Fokker-Planck modeling of the fast α-particle transport and collisional relaxation. A specific formalism, based on a two-scale approach with respect to

energy is then introduced in Section 3. It provides a self-consistent modeling of the coupling between suprathermal and thermal plasma species. Section 4 presents the algorithms devised to solve the two-scale coupling. A finite volume method is applied to the Fokker-Planck equation governing the suprathermal α-particle distribution function. Fast algorithms are then specially optimized to solve the discretized model efficiently. Section 5 presents some numerical results regarding the α-particle distribution function evolution and its coupling with the thermal bulk. We show how the methods developed here provide a refined description of the thermalization process. Simulations are carried out in conditions relevant for typical ICF targets. Conclusions are finally presented in Section 6.

2. Physical model for the transport and collisional relaxation of α-particles

Once created by fusion reactions, suprathermal α-particles are transported through an inhomogeneous plasma and slowed down through Coulomb collisions with electrons and thermal D,T ions. Besides, pressure gradients give rise to an electrostatic field $\vec{\mathcal{E}}(\vec{r},t)$ that may accelerate or decelerate α-particles. To give an accurate description of the particle transport, as well as the non-local energy and momentum exchange that occur between α-particles and the thermal bulk, a kinetic modeling based on the Vlasov-Fokker-Planck equation is required.

2.1. Vlasov-Fokker-Planck equation for the α-particles

The distribution function $f_\alpha(\vec{r},\vec{v},t)$ of α-particles characterized by a charge $Z_\alpha e$ and a mass m_α is governed by the Vlasov-Fokker-Planck equation:

$$\frac{\partial f_\alpha}{\partial t} + \vec{v}\cdot\frac{\partial f_\alpha}{\partial \vec{r}} + \frac{Z_\alpha e\vec{\mathcal{E}}}{m_\alpha}\cdot\frac{\partial f_\alpha}{\partial \vec{v}} = \sum_i \left.\frac{\partial f_\alpha}{\partial t}\right|_{\alpha i} + \left.\frac{\partial f_\alpha}{\partial t}\right|_{\alpha e} + \left.\frac{\partial f_\alpha}{\partial t}\right|_{\text{fuse}}. \tag{1}$$

The first two terms on the right hand side of this equation describe the collisional relaxation of α-particles:

- $\partial f_\alpha/\partial t|_{\alpha e}$ stands for the collisions of α-particles with electrons,
- $\sum_i \partial f_\alpha/\partial t|_{\alpha i}$ describes the collisions of α-particles with thermal ion species. Since thermal species densities are significantly higher than the fast α-particle density (at least at the beginning of the ignition and burn processes), the non-linear term corresponding to fast-α/fast-α scattering is neglected. The coupling between the thermalized α-particles and the suprathermal ones is naturally included.

We focus now on the collisional part of Eq. (1). The Vlasov part of the equation modeling the transport in space and the acceleration due to the electrostatic field is considered separately in Section 4. In a fully ionized plasma such as the one considered here, large angle scattering is much less likely than the net large-angle deflection due to a cumulative effect of many small-angle collisions that the projectile experiences along its path [15]. Each of the collision terms in right hand side of Eq. (1) can then be expressed as a Fokker-Planck operator in velocity space, which amounts essentially to an advection-diffusion form. More precisely, the slowing down of α-particles on a thermal ion species i can be written as:

$$\left.\frac{\partial f_\alpha}{\partial t}\right|_{\alpha i} = 4\pi\Gamma_{\alpha i}\frac{\partial}{\partial \vec{v}}\cdot\left(\frac{m_\alpha}{m_i}f_\alpha\frac{\partial \mathcal{S}_i}{\partial \vec{v}} - \nabla_v^2\mathcal{T}_i\cdot\frac{\partial f_\alpha}{\partial \vec{v}}\right), \tag{2}$$

where $\mathcal{S}_i$ and $\mathcal{T}_i$ are the so-called Rosenbluth potentials [15] associated to the target ions i. They are defined by a set of Poisson equations in velocity space:

$$\Delta_v\mathcal{S}_i = f_i, \qquad \Delta_v\mathcal{T}_i = \mathcal{S}_i. \tag{3}$$

The coefficient $\Gamma_{\alpha i} = (4\pi Z_\alpha^2 Z_i^2 e^4/m_\alpha^2)\ln\Lambda_{\alpha i}$ is proportional to the Coulomb logarithm $\ln\Lambda_{ij}$ (for any species i,j including electrons) related to the Coulomb potential screening and taking quantum effects into account: $\Lambda_{ij} = \lambda_D/\max\{\lambda_{\text{bar}},\rho_\perp\}$. The Debye length

$$\lambda_D = \left(4\pi n_e e^2/T_e + \sum_{j=1}^{n} 4\pi n_j Z_j^2 e^2/T_j\right)^{-1/2}$$

depends on the temperature T_j, which is expressed in energy units. T_j is related to the thermal ion distribution function f_j by the relation:

$$T_j = \frac{m_j}{3n_j} \int (v - V_j)^2 f_j(\vec{v})\, d^3v,$$

where $n_j = \int f_j(\vec{v})\, d^3v$ is the density of ion species j and $\vec{V}_j = n_j^{-1} \int \vec{v} f_j(\vec{v})\, d^3v$ is their mean velocity. The characteristic lengths $\rho_\perp$ and λ_{bar} are the classical and quantum impact parameters:

$$\rho_\perp = Z_a Z_b e^2 / m_{ij} u_{ij}^2, \qquad \lambda_{\text{bar}} = \hbar / m_{ij} u_{ij}$$

where $m_{ij} = m_i m_j/(m_i + m_j)$ is the reduced mass and $u_{ij} = \sqrt{3}(T_i/m_i + T_j/m_j)^{1/2}$ is an average relative velocity between the particle species i and j. The Coulomb logarithm is thus a particular function of hydrodynamic quantities. It is also symmetric with respect to particle species, $\Lambda_{ij} = \Lambda_{ji}$, which is related to energy and momentum conservation during the collision.

The effect of electrons on the slowing down of α-particles is modeled by another Fokker-Planck term, in which the electron distribution function is approximated by a Maxwellian characterized by a density n_e, a mean velocity $\vec{u}_e$ and a temperature T_e:

$$\left.\frac{\partial f_\alpha}{\partial t}\right|_{\alpha e} = \frac{1}{\tau_{e\alpha}} \frac{\partial}{\partial \vec{v}} \cdot \left[(\vec{v} - \vec{u}_e) f_\alpha(\vec{v}) + \frac{T_e}{m_\alpha} \frac{\partial f_\alpha}{\partial v_\alpha}(\vec{v}) \right], \tag{4}$$

where $\tau_{e\alpha}$ is a characteristic $e - \alpha$ collision time defined by:

$$\tau_{e\alpha} = \frac{3}{4\sqrt{2\pi}} \frac{m_\alpha T_e^{3/2}}{n_e Z_\alpha^2 e^4 m_e^{1/2} \ln \Lambda_{\alpha e}}. \tag{5}$$

Equation (4) is obtained by a truncated expansion of the full ion-electron Fokker-Planck operator with respect to the small constant $\epsilon = (m_e/m_i)^{1/2} \sim 0.022$ [4, 6].

The last term in (1) stands for the creation of α-particles by fusion reactions. The source term is supposed to be isotropic and is given by:

$$\left.\frac{\partial f_\alpha}{\partial t}\right|_{\text{fuse}} = \mathcal{R}_{DT}(\vec{r}, t) \frac{\delta(v - v_h)}{4\pi v^2}, \tag{6}$$

where $v_h = 1.3 \times 10^9\,\text{cm.s}^{-1}$ is the initial velocity of suprathermal α-particles whose initial energy is 3.52 MeV. $\mathcal{R}_{DT}$ is the fusion reaction rate expressed as a function of the distribution functions of D and T, respectively:

$$\mathcal{R}_{DT}(\vec{r}, t) = n_D n_T \langle \sigma v \rangle_{DT} = \int\int f_D(\vec{r}, \vec{v}_D, t)\, f_T(\vec{r}, \vec{v}_T, t)\, |\vec{v}_D - \vec{v}_T|\, \sigma_{DT}(|\vec{v}_D - \vec{v}_T|)\, d^3v_D d^3v_T. \tag{7}$$

The distribution functions f_D and f_T are solutions of the Vlasov-Fokker-Planck equation written on the deuterium and tritium species, respectively, and they are not necessarily Maxwellian functions. Integrals in Eq. (7) are taken over the three-dimensional velocity space.

2.2. Dealing with electrons

The coupling between the electron fluid model and the ion kinetic model is well known [16]. For the sake of completeness, we show how the electron fluid model is adapted to the two-scale ion kinetic approach. Since the characteristic time of the considered problem is close to the ion-ion collision time $\tau_{ii} >> 1/\omega_{pe}$, ω_{pe} being the electron plasma frequency, and the characteristic length is of the order of the ion collisional mean free path $\lambda_i >> \lambda_{De}$, λ_{De} being the electron Debye length, the quasi-neutrality assumption is relevant. We then have:

$$n_e = \sum_i Z_i n_i + Z_\alpha n_\alpha^{ST}, \qquad \vec{V}_e = \sum_i Z_i n_i \vec{V}_i + Z_\alpha n_\alpha^{ST} V_\alpha^{ST}, \tag{8}$$

where the contribution of suprathermal α-particles is naturally included, $n_\alpha^{ST}, V_\alpha^{ST}$ being the density and mean velocity of fast α-particles respectively.

Besides, due to a very small ratio of the masses of electrons and ions, the electron equilibration time τ_{ee} is significantly smaller than the mean ion-ion collision time τ_{ii}. According, for example to [17], we have the following ordering of characteristic times: $\tau_{ee} \sim \epsilon\tau_{ii}$. As a consequence, the electron kinetic equation reduces to a fluid equation. Only an equation for the temperature (or, equivalently, the energy density) is actually needed since the electron density and velocity are known from the quasi-neutrality conditions (8).

In the one-dimensional spherical problem considered here, the electron energy density W_e is governed by the following conservation equation :

$$\frac{\partial W_e}{\partial t} + \frac{1}{r^2}\frac{\partial}{\partial r}\left(r^2 u_e W_e\right) + \frac{1}{r^2}\frac{\partial}{\partial r}(r^2 u_e)P_e - \frac{1}{r^2}\frac{\partial}{\partial r}\left(r^2\kappa_e\frac{\partial T_e}{\partial r}\right) = \sum_{j=1}^{n}\frac{3n_j}{2\tau_{ej}}(T_j - T_e) + \left.\frac{\partial W_e}{\partial t}\right|_{\rm rad} \tag{9}$$

where κ_e is Spitzer's thermal conductivity [18] in the presence of several ion species (see also [19] and Appendix in [20]). In practice, we apply a flux limiter $f = 0.05$ on the electron heat flux to make sure that it remains below the free-streaming limit. Besides, we control that the unlimited flux always remains small compared to the free streaming flux, so that the artificial flux limitation is relevant. The ratio between the unlimited and free streaming flux never exceeds 0.15 during the whole process of implosion. At the end of implosion and during the combustion, the ratio is less than 0.05, so that the use of the limiter $f = 0.05$ is reasonable for the considered problem.

The collision time τ_{ej} has been defined in Eq. (5) where α is replaced by the considered ion species j. The electron energy density W_e and pressure P_e are given by an equation of state taking into account Fermi degeneracy [6].

The last term on the right hand side of (9) accounts for the radiation losses of electrons.

2.3. Relative importance of electrons and ions on the slowing down of α-particles

3.52 MeV α-particles are created in fusion reactions isotropically, in the system of reference associated with the thermal bulk. Then, they are slowed down through Coulomb collisions with electrons, according to Eq. (4), and with thermal ions, according to Eq. (2). The relative importance of electrons and ions on the slowing down of α-particles can be estimated by retaining only the dynamical friction terms from the Fokker-Planck equations (4) and (2). The ratio $R_{i/e}$ between the ion slowing down and the electron one can thus be approximated by:

$$R_{i/e} = \left.\frac{\partial f_\alpha}{\partial t}\right|_{\alpha i} \Big/ \left.\frac{\partial f_\alpha}{\partial t}\right|_{\alpha e} \sim \frac{T_e^{3/2}}{v^3 m_e^{1/2} m_i} \sim \frac{T_e^{3/2}}{v^3 m_i^{3/2}\epsilon}.$$

The ratio $R_{i/e}$ is thus defined by a characteristic threshold velocity:

$$v_c = \epsilon^{-1/3}(T_e/m_i)^{1/2}, \tag{10}$$

so that $R_{i/e} \sim (v_c/v)^3$.

The beginning of the slowing-down of α-particles is thus governed nearly exclusively by electrons. Then, as $v \sim v_c$, the effect of ions and electrons on the α relaxation become comparable. Eventually, the final stage of α-particle thermalization is essentially influenced by collisions with thermal ions. Supposing $T_i \sim T_e$, we have the following estimate $v_c \sim \epsilon^{-1/3} v_i^{th} \sim 3.6\, v_i^{th}$, v_i^{th} being the typical thermal velocity of D and T ions. The effect of thermal ions on the α relaxation dominates when the α velocity is below $v_c \sim 3.6\, v_i^{th}$. We shall refer to such α-particles as "moderately suprathermal".

3. Two-component description of the α distribution function

3.1. Physical discussion

From the previous discussion, we know that 3.52 MeV α-particles are firstly slowed down essentially by electrons. The first stage of the α slowing down is thus described by:

$$\left.\frac{\partial f_\alpha}{\partial t}\right|_{\rm coll} = \frac{1}{\tau_{\alpha e}}\frac{\partial}{\partial \vec{v}}\cdot\left[(\vec{v} - \vec{u}_e)f_\alpha(\vec{v}) + \frac{T_e}{m_\alpha}\frac{\partial f_\alpha}{\partial \vec{v}}(\vec{v})\right]. \tag{11}$$

When $v >> u_e$, the dynamic friction term (first term on the right hand side of (11)) dominates so that the α distribution evolves with respect to:

$$\left(\frac{\partial f_\alpha}{\partial t}\right)_{coll} \approx \frac{1}{\tau_{\alpha e}}\frac{1}{v^2}\frac{\partial}{\partial v}\cdot\left[v^3 f_\alpha(v)\right]. \tag{12}$$

The stationary solution of (12) behaves as $f_\alpha \sim 1/v^3$, where v is the suprathermal α-particle velocity. Consequently, as long as fast α-particles remain far from the thermal velocity region, their distribution function varies smoothly over the whole suprathermal velocity region. The associated velocity scale v_α^{ST}, defined by:

$$v_\alpha^{ST} \sim f_\alpha^{ST}/\frac{\partial f_\alpha^{ST}}{\partial v}, \tag{13}$$

is in particular greater than the target thermal velocity $v_i^{th} = (T_i/m_i)^{1/2}$.

Then, when slowed down α-particles get closer to the thermal region but still remain suprathermal, thermal ions tend to dominate the end of the relaxation process, which is then governed by the equation:

$$\left.\frac{\partial f_\alpha}{\partial t}\right|_{\rm coll} = \sum_i 4\pi\Gamma_{\alpha i}\frac{\partial}{\partial\vec{v}}\cdot\left(\frac{m_\alpha}{m_i}f_\alpha\frac{\partial\mathcal{S}_i}{\partial\vec{v}}\right), \tag{14}$$

where only the dynamical friction term is retained for the present discussion. We shall deal with the diffusion part separately. Qualitatively, for suprathermal α-particles, one can consider that the distribution function of the thermal target species i appears highly localized in velocity space. One thus can write: $f_i(\vec{v}) = n_i\delta^3(\vec{v})$ (assuming that the mean velocity is zero). Besides, the divergence with respect to velocity that appears on the right hand side of Eq. (14) can be expanded as follows:

$$\frac{\partial}{\partial\vec{v}}\cdot\left(\frac{\partial\mathcal{S}_i}{\partial\vec{v}}f_\alpha\right) \simeq \frac{\partial\mathcal{S}_i}{\partial\vec{v}}\cdot\frac{\partial f_\alpha}{\partial\vec{v}} + f_\alpha\Delta_v\mathcal{S}_i.$$

Using the approximation $f_i(\vec{v}) = n_i\delta^3(\vec{v})$, which is valid for suprathermal α-particles, the first Rosenbluth potential associated to the target ions i can be calculated explicitly: $\mathcal{S}_i(v) \sim -n_i/(4\pi v)$. Then, by calculating its derivative, the slowing down of α-particles can be modeled by:

$$\left.\frac{\partial f_\alpha}{\partial t}\right|_{\rm coll} = \sum_i 4\pi\Gamma_{\alpha i}\frac{m_\alpha}{m_i}\left(\frac{\partial f_\alpha}{\partial\vec{v}}\cdot\frac{n_i}{4\pi v^2}\vec{e}_v + f_\alpha f_i\right). \tag{15}$$

The two terms on the right hand side of Eq.(15) have a clear physical sense. The first term $\sim \partial f_\alpha/\partial\vec{v}$ varies slowly and smoothly far from the thermal velocity region. It can be characterized by a suprathermal velocity scale v_α^{ST}, which is greater than the typical thermal ion velocity v_i^{th}. Actually, the term $\sim \frac{n_i}{4\pi v^2}\frac{\partial f_\alpha}{\partial\vec{v}}$ corresponds to a conservative convection towards $v = 0$. The associated convective rate $\frac{n_i}{4\pi v^2}$ increases as v tends to 0 so that the solution of:

$$\left(\frac{\partial f_\alpha}{\partial t}\right)_{coll} = \sum_i 4\pi\Gamma_{\alpha i}\frac{m_\alpha}{m_i}\left[\frac{\partial f_\alpha}{\partial\vec{v}}\cdot\frac{n_i}{4\pi v^2}\vec{e}_v\right] \tag{16}$$

tends to a constant f_0 corresponding to the stationary state of (16). The part of the α distribution driven by (16) is then stretched and smoothed out as it approaches the thermal velocity region.

The second term $\sim f_\alpha f_i$ appears highly localized in the thermal region of velocity space and behaves qualitatively as a δ-function for suprathermal α-particles. This term actually leads to the formation of a condensate of width $v_i^{th} \ll v_\alpha^{ST}$.

This qualitative analysis shows intuitively how the *two-component feature* of the α distribution function builds up. It is made of a superposition of two components evolving on two different velocity scales, namely:

- a suprathermal component, fed by fusion reactions and evolving on a large velocity scale, greater than the target thermal velocity.

- A thermal component, corresponding to the thermalized part of the α distribution function, evolving on the same velocity scale as the thermal bulk of the plasma. Note that this component is not fully thermalized since the source term is proportional to $\sum_i 4\pi\Gamma_{\alpha i} f_i$. There remains a final stage of collisional relaxation between the thermal components of D,T and α ions respectively.

Fig. 1 illustrates schematically those processes. From this phenomenological discussion, we can draw a more formal and more rigorous description of the slowing-down which naturally leads to the building of a new multi-scale algorithm solving the initial problem given by Eq. (1).

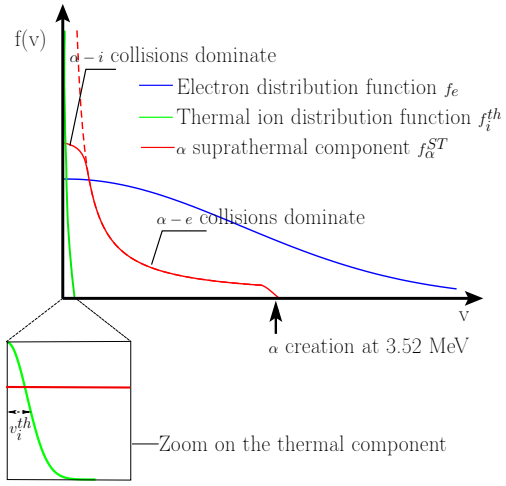

Figure 1: Schematic representation of the collisional relaxation of suprathermal α-particles on thermal target ions i. The suprathermal component of the α distribution (red) varies on the velocity scale $v_\alpha^{ST} \gg v_i^{th}$. The electron distribution function (blue) has a Maxwellian shape with a characteristic width $v_e^{th} \gg v_i^{th}$. The thermal ion component (green) varies on the thermal ion energy scale $\sim v_i^{th}$. On that scale, the suprathermal component appears almost constant. The red broken line refers to the stationary solution of Eq. (12). The solution corresponding to the collisional relaxation of suprathermal particles on electrons behaves as $\sim 1/v^3$. The divergence as $v \to 0$ is cut off by the effect of thermal ions that dominate the end of the relaxation process. For the suprathermal component, this final relaxation corresponds to a convection in velocity space, such that the distribution function appears almost constant on the thermal velocity scale according to Eq. (16).

3.2. Splitting of the Fokker-Planck operator

Using the well-known temperature vanishing form of the Rosenbluth potentials [15], it is possible to rearrange the terms of the Fokker-Planck equation, leading to the description of the α distribution function by a set of 2 components, such that:

$$f_\alpha(\vec{v}, t) = f_\alpha^{ST}(\vec{v}, t) + f_\alpha^{T}(\vec{v}, t), \tag{17}$$

where: f_α^{ST} denotes the suprathermal component. It is defined on a large velocity domain, spreading to the MeV range. Its typical velocity variation scale v_α^{ST} is greater than the thermal ion velocity v_i^{th}; f_α^{T} is the thermal component. It is localized in the region of velocity space corresponding to target thermal ion distribution functions and vanishes in the suprathermal velocity domain. The component f_α^{T} is designed to describe accurately the final stage of thermalization of the slowed down α-particles. This final relaxation occurs on a velocity scale $\sim v_i^{th}$.

Let us emphasize that the two components defined in Eq. (17) do exist in the whole velocity space, the relevant physical quantity being the full α distribution function $f_\alpha(\vec{v}, t)$.

The idea is then to deal with each component separately. The original Fokker-Planck operator given in Eq. (2) is then transformed into a *system of two coupled equations* governing the two components f_α^{ST} and f_α^{T}, respectively:

$$\begin{aligned}
\partial_t f_\alpha^{ST}\big|_{\alpha i} &= \Gamma_{\alpha i} \frac{n_i}{v^2} \partial_v f_\alpha^{ST} - n_i \Gamma_{\alpha i} f_\alpha^{ST} \frac{\delta(v)}{v^2}, \\
\partial_t f_\alpha^{T}\big|_{\alpha i} &= 4\pi\Gamma_{\alpha i} \partial_{\vec{v}} \cdot \left(f_\alpha^{T} \partial_{\vec{v}} \mathcal{S}_i \right) + 4\pi\Gamma_{\alpha i} f_i f_\alpha^{ST}(v = 0).
\end{aligned} \tag{18}$$

The above equations are written in the system of reference associated with the thermal ions. The subscript i denotes every thermal distributions, including the thermalized α distribution function.

System (18) describes the coupling between the suprathermal component and the thermal one, the coupling function being $\sim f_\alpha^{ST} f_i$, which is subtracted from the equation on the suprathermal component f_α^{ST} and appears as a source term in the equation governing the thermal component f_α^T. The coupling function can actually be approximated for each of the components of the α distribution function in two different ways, depending on the considered velocity scale:

- For the suprathermal component, we have $f_\alpha^{ST} f_i \sim n_i f_\alpha^{ST} \delta^3(\vec{v})$ since thermal target ions appear highly localized.
- For the thermal component, we can consider $f_\alpha^{ST} f_i \sim f_\alpha^{ST}(0) f_i$ since the suprathermal component is almost constant on the thermal velocity scale v_i^{th}. The term $\sim f_\alpha^{ST}(0) f_i$ appears as a source term for the thermal component. It corresponds to a feeding by the suprathermal component.

In Eq. (18), we have disregarded the process corresponding to a feeding of the suprathermal component by the thermal one, which could be the case if we modeled large angle collisions, such as $\alpha^{ST} + D \to \alpha + D^{ST}$. Such collisions would build up a suprathermal component for species D and T. This could be naturally included in the formalism that we describe here, but this is a process of second order since the probability of large angle scattering is $\sim 1/\ln\Lambda$ times smaller than the small-angle collisions modeled by the Fokker-Planck operator.

3.3. Diffusion part of the Fokker-Planck operator

We study now the effect of the second term on the right hand side of Eq. (2) corresponding to a diffusion in velocity:

$$\left.\frac{\partial f_\alpha}{\partial t}\right|_{\alpha i} = -\sum_i 4\pi\Gamma_{\alpha i} \frac{\partial}{\partial \vec{v}} \cdot \left(\nabla_v^2 \mathcal{T}_i \cdot \frac{\partial f_\alpha}{\partial \vec{v}} \right). \tag{19}$$

$\mathcal{T}_i$ is the second Rosenbluth potential associated to the thermal target ions. The notation $\nabla_v^2(\,.\,)$ stands for the Hessian $\partial^2_{\alpha\beta}(\,.\,)$. Let us define the field $\vec{J}_{\alpha i}$, representing the slowing-down current of suprathermal α-particles:

$$\vec{J}_{\alpha i} = -\sum_i 4\pi\Gamma_{\alpha i} \nabla_v^2 \mathcal{T}_i \partial f_\alpha / \partial \vec{v}, \tag{20}$$

Using the Dirac-function approximation for the thermal target distribution functions, we can approximate $\mathcal{T}_i$ by its temperature-vanishing form, $\mathcal{T}_i(v) \sim -n_i v/(8\pi)$. The approximation is relevant for the suprathermal component. The Hessian $\nabla_v^2 \mathcal{T}_i$ can then be calculated explicitly:

$$\nabla_v^2 \mathcal{T}_i \sim -\frac{n_i}{8\pi v} \left(\mathrm{Id} - \frac{\vec{v} \otimes \vec{v}}{v^2} \right). \tag{21}$$

By taking advantage of a polar representation of the velocity $\vec{v} = v\vec{e}_v$, where $(\vec{e}_v, \vec{e}_\theta)$ is the polar local basis of velocity space, the Hessian (21) simplifies to:

$$\nabla_v^2 \mathcal{T}_i \sim -\frac{n_i}{8\pi v}\, \vec{e}_\theta \otimes \vec{e}_\theta\,. \tag{22}$$

The slowing down current defined in Eq. (20) expresses the diffusion in velocity associated to the slowing-down process. It is essentially transverse, that is, perpendicular to the local velocity $\vec{v}$. Therefore, one can write:

$$\vec{J}_{\alpha i} \sim -\frac{\Gamma_{\alpha i}}{2} \frac{n_i}{v^2} \frac{\partial f_\alpha}{\partial \theta} \vec{e}_\theta. \tag{23}$$

The diffusive slowing-down current is thus highly anisotropic in velocity space and it intensifies as α-particles approach the thermal bulk region of velocity space. Qualitatively, the collisional relaxation of α-particles on thermal target ions is thus characterized by:

- a pure advection in velocity space at a constant rate, modeled by Eq. (14), which tends to accumulate α-particles in the thermal ion velocity region.
- An anisotropic diffusion in velocity space, expressed by Eq. (23), which tends to make the distribution isotropic when slowed-down α-particles get closer to the final stage of thermalization.

4. Algorithms for the transport and collisional relaxation of fast fusion products

In this section, we present the numerical methods developed to solve Eq. (1) and Eq. (18). Those equations govern the time evolution of suprathermal α-particles. Firstly, we show how to deal with the two-component nature of the α distribution function. We then develop a finite volume approach to discretize the equation on the α suprathermal component. An efficient explicit algorithm is then applied to model the time evolution of the suprathermal component with relatively low computational time. We finally present how to accurately simulate the complete thermalization process of α-particles.

4.1. Co-existence of two velocity grids

The two-component nature of the α distribution function naturally leads to the co-existence of two velocity grids, namely:

- A suprathermal grid, designed to represent the evolution of the suprathermal component of the α distribution function f_α^{ST}. It covers a large domain in velocity, extending to the range $v \simeq v_h \simeq 1.3 \times 10^9$ cm/s, which is the velocity corresponding to the α-particles created by fusion reactions. Moreover, since the suprathermal component varies smoothly, we can use a relatively coarse grid to discretize it. The suprathermal grid has to be fine enough to resolve the structures drawn by the the suprathermal component f_α^{ST}. The resolution is thus independent of the local thermal ion temperature. In practice, it is convenient to choose a resolution which is of the order of one typical hot spot thermal velocity v_i^{th}. This choice ensures an accurate description of the suprathermal component variations which occur on a velocity scale $v_\alpha^{ST} \gg v_i^{th}$ (see, for instance Fig. 16) and is such that f_α^{ST} is almost constant on the thermal velocity support.
- A thermal grid, on which the thermal component of the α distribution f_α^{T} is discretized. This grid is designed to capture the final stage of collisional relaxation of the almost-thermalized component of the α distribution on the other thermal ion species D and T. This process entails a velocity resolution much smaller than the local thermal velocity scale v_i^{th}. The thermal grid makes use of a cylindrical parametrization $(v_r, v_\perp)$ inherited from the code FPION [19].

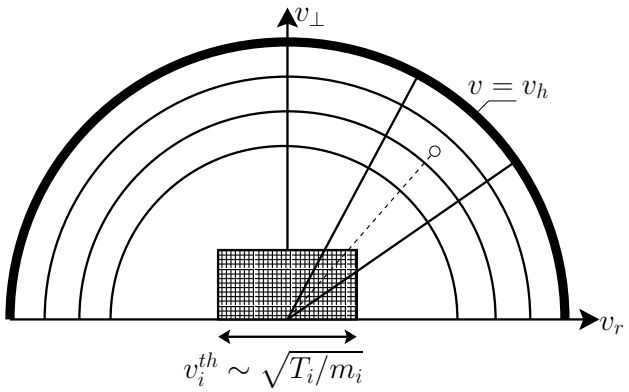

Figure 2: Schematic representation of the two velocity grids used to model the α suprathermal and thermal components respectively. The suprathermal component evolves on the coarse polar grid, covering a wide domain extending to the MeV region. The thick shell of width $\sim T_i$ corresponds to the source term due to fusion reactions. The thermal component evolves on the small and refined cylindrical grid. Both meshes are centered on the mean local bulk velocity $V_0 \sim V_e \sim V_i$. Velocity space is characterized by an axial symmetry around the axis $\vec{v}_r$.

The two grids that are shown in Fig. 2 are centered on the local mean bulk velocity $V_0(r)$, which is close to the mean electron velocity $V_e(r)$. By using two grids specially-tailored to capture the variations of each component, it is possible to build an efficient algorithm modeling the two components of the α distribution.

4.2. Dimensionless form of the Vlasov-Fokker-Planck equation

For numerical purposes, we write the Vlasov-Fokker Planck equation governing the evolution of the suprathermal component of the α distribution function f_α^{ST} in a dimensionless form, based on a specified unit system given in Table 1. It is chosen to manipulate numbers that are close to unity. This prevents computational errors caused by under or overflow floating numbers. As it was shown in Eq. (23), the collision term between suprathermal α-particles and ions takes a simple form expressed in polar coordinates. The slowing down currents are co-linear with the local polar basis vectors $\vec{e}_v, \vec{e}_\theta$ of velocity space. In the spherical one-dimensional geometry considered here, it thus seems natural to parametrize the suprathermal distribution function as $f_\alpha^{ST}(r, v, \theta, t)$, with two velocity components $\vec{v} = v\cos\theta\,\vec{e}_r + v\sin\theta\,\vec{e}_\perp$. Then, the dimensionless equation governing f_α^{ST} reads:

$$\frac{\partial f_\alpha^{ST}}{\partial t} + v\,\cos\theta\,\frac{\partial f_\alpha^{ST}}{\partial r} + \frac{\mathcal{E}_\alpha}{A_\alpha}\cos\theta\frac{\partial f_\alpha^{ST}}{\partial v} = \sum_i \widetilde{\Gamma}_{\alpha i}\frac{\partial}{\partial \vec{v}}\cdot\left[\frac{n_i}{v^2}\left(\frac{A_\alpha}{A_i}f_\alpha^{ST}\vec{e}_v + \frac{1}{2}\frac{\partial f_\alpha^{ST}}{\partial\theta}\vec{e}_\theta\right)\right]$$
$$+\frac{1}{\widetilde{\tau}_{e\alpha}}\frac{\partial}{\partial\vec{v}}\cdot\left[(\vec{v}-\vec{u_e})f_\alpha^{ST} + \frac{T_e}{A_\alpha}\frac{\partial}{\partial\vec{v}}f_\alpha^{ST}\right] - \sum_{i=D,T,\alpha} 4\pi\widetilde{\Gamma}_{\alpha i}\frac{A_\alpha}{A_i}f_\alpha^{ST}f_i^T + \mathcal{R}_{DT}(\vec{r},t)\frac{\delta(v-v_h)}{4\pi v^2}, \tag{24}$$

where the normalized constant $\widetilde{\Gamma}_{\alpha i} = (4\pi Z_\alpha^2 Z_\beta^2/A_i^2)\ln\Lambda_{\alpha i}$ and the effective electrostatic field $\mathcal{E}_i$ applied to ions of species i is defined by the following expression:

$$\mathcal{E}_i = -(Z_i/\widetilde{n}_e)\,\partial\widetilde{P}_e/\partial r. \tag{25}$$

Here, $\widetilde{n}_e$ and $\widetilde{P}_e$ are the dimensionless electron density and pressure, respectively, and

$$\widetilde{\tau}_{e\alpha} = \frac{3\sqrt{\pi}A_\alpha T_e^{3/2}}{2\epsilon\sqrt{2}Z_\alpha^2 n_e\ln\Lambda_{\alpha e}}$$

is the dimensionless electron-ion collision time.

Table 1: Units defined from reference values of the particle density n_0 and particle thermal energy T_0.

Quantity	Unit
density	n_0 (arbitrary reference value)
thermal energy	T_0 (arbitrary reference value)
time	$\tau_0 = T_0^{3/2}m_p^{1/2}/4\pi e^4 n_0$
length	$\lambda_0 = (T_0/m_p)^{1/2}\tau_0 = T_0^2/4\pi e^4 n_0$
velocity	$v_0 = (T_0/m_p)^{1/2} = \lambda_0/\tau_0$
distribution function	$f_0 = n_0/v_0^3$
first Rosenbluth pot.	$\mathcal{S}_0 = n_0/v_0$
second Rosenbluth pot.	$\mathcal{T}_0 = n_0 v_0$
electric field ($\mathcal{E}_i$)	$\mathcal{E}_0 = m_p v_0^2/\lambda_0 = m_p\lambda_0/\tau_0^2$
heat flux	$Q_0 = n_0 T_0^{3/2}/m_p^{1/2}$

Let us consider the third term on the right hand side of (24). For suprathermal α-particles, it can be approximated by:

$$\sum_i 4\pi\widetilde{\Gamma}_{\alpha i}\frac{A_\alpha}{A_i}f_\alpha^{ST}f_i \simeq 4\pi\sum_i\widetilde{\Gamma}_{\alpha i}\frac{A_\alpha}{A_i}f_\alpha^{ST}n_i\delta^3(\vec{v}), \tag{26}$$

supposing that $v \gg v_i^{th}, V_0$. The term (26) is thus highly peaked with respect to velocity in the thermal component region and leads to the formation of a thermalized condensate that cannot be described on the coarse suprathermal grid. That justifies our approach of subtracting this singular term from (24), so that the variations of f_α^{ST} remain

everywhere smooth and may be described on the suprathermal grid. The term (26) is then re-introduced as a *feeding term* in the equation governing the thermal component, so that the original Fokker-Planck equation governing the complete α distribution function $f_\alpha = f_\alpha^{ST} + f_\alpha^{T}$ is recovered.

To solve the full Vlasov-Fokker-Planck equation (24), we use the same general splitting scheme as in the code Fpion, namely we treat the advection, the acceleration and the collisional stages separately. We describe now the method developed to solve the collisional part of (24).

4.3. Discretization of the collisional term

The collisional part of (24) can be written as:

$$\left.\frac{\partial f_\alpha^{st}}{\partial t}\right|_{\text{coll}} = \frac{1}{v^2}\frac{\partial}{\partial v}\left(v^2 J^v\right) + \frac{1}{v\sin\theta}\frac{\partial}{\partial\theta}\left(\sin\theta\, J^\theta\right), \tag{27}$$

where the polar components of the slowing down current $\vec{J}$ are given by:

$$J^v = f_\alpha^{ST}\left(\frac{v}{\tau_{e\alpha}} + \widetilde{\Gamma}_{\alpha i}\frac{A_\alpha}{A_i}\frac{n_i}{v^2}\right) + \frac{1}{\widetilde{\tau}_{e\alpha}}\frac{T_e}{A_\alpha}\frac{\partial f_\alpha^{ST}}{\partial v}, \tag{28}$$

and

$$J^\theta = \frac{1}{v}\frac{\partial f_\alpha^{ST}}{\partial\theta}\left(\widetilde{\Gamma}_{\alpha i}\frac{n_i}{2v} + \frac{1}{\widetilde{\tau}_{e\alpha}}\frac{T_e}{A_\alpha}\right), \tag{29}$$

The slowing-down current $\vec{J}$ takes the general advection-diffusion form in velocity space:

$$\begin{pmatrix} J^v \\ J^\theta \end{pmatrix} = f\begin{pmatrix} u_v \\ u_\theta \end{pmatrix} + \begin{pmatrix} K^{vv} & K^{v\theta} \\ K^{\theta v} & K^{\theta\theta} \end{pmatrix}\cdot\begin{pmatrix} \dfrac{\partial f}{\partial v} \\ \dfrac{1}{v}\dfrac{\partial f}{\partial\theta} \end{pmatrix} \tag{30}$$

where the components of the tensors u and K are related to the Rosenbluth potentials $\mathcal{S}$ and $\mathcal{T}$ (associated to the target ion species) as follows:

$$\begin{pmatrix} u^v \\ u^\theta \end{pmatrix} = \begin{pmatrix} \dfrac{\partial\mathcal{S}}{\partial v} \\ \dfrac{1}{v}\dfrac{\partial\mathcal{S}}{\partial\theta} \end{pmatrix} \quad \text{and} \quad \begin{pmatrix} K^{vv} & K^{v\theta} \\ K^{\theta v} & K^{\theta\theta} \end{pmatrix} = \begin{pmatrix} \dfrac{\partial^2\mathcal{T}}{\partial v^2} & \dfrac{\partial}{\partial v}\left(\dfrac{1}{v}\dfrac{\partial\mathcal{T}}{\partial\theta}\right) \\ \dfrac{\partial}{\partial v}\left(\dfrac{1}{v}\dfrac{\partial\mathcal{T}}{\partial\theta}\right) & \dfrac{1}{v^2}\dfrac{\partial^2\mathcal{T}}{\partial\theta^2} + \dfrac{1}{v}\dfrac{\partial\mathcal{T}}{\partial v} \end{pmatrix}$$

which reduces to:

$$\begin{pmatrix} u^v \\ u^\theta \end{pmatrix} = \begin{pmatrix} v/\widetilde{\tau}_{e\alpha} + \sum_{i=D,T}\widetilde{\Gamma}_{\alpha i}n_i/v^2 \\ 0 \end{pmatrix} \quad \text{and} \quad \begin{pmatrix} K^{vv} & K^{v\theta} \\ K^{\theta v} & K^{\theta\theta} \end{pmatrix} = \begin{pmatrix} T_e/\widetilde{\tau}_{e\alpha}A_\alpha & 0 \\ 0 & \sum_{i=D,T}\widetilde{\Gamma}_{\alpha i}n_i/(2v) \end{pmatrix}. \tag{31}$$

Note the simplifications implied by using a polar parametrization of velocity space: the dynamical friction coefficient $\vec{u}$ is indeed co-linear with the radial velocity basis vector $\vec{e}_v$ and the diffusion tensor is diagonal in the basis $\vec{e}_v, \vec{e}_\theta$.

We then integrate (27) with respect to velocity on a given cell δV_{kj} of the polar suprathermal velocity grid, subscripts k and j referring to the θ and v directions respectively (see figure 3).

The cell δV_{kj} is defined by its boundaries $\theta_{k-\frac{1}{2}}$, $\theta_{k+\frac{1}{2}}$ and $v_{j-\frac{1}{2}}$, $v_{j+\frac{1}{2}}$, for $1 \le k \le k_{max}$ and $1 \le j \le j_{max}$. We call $f_{kj}^n = f_\alpha^{ST}(v = v_j, \theta = \theta_k, t = t_n)$ the value of the suprathermal distribution function in the cell δV_{kj} at time t_n. Integrating Eq. (27) over the cell area δV_{kj}, we obtain the following conservative discretized form:

$$\frac{f_{kj}^{n+1} - f_{kj}^n}{\Delta t} = \frac{1}{v_j^2}\frac{v_{j+1/2}^2 J_{kj+1/2}^v - v_{j-1/2}^2 J_{kj-1/2}^v}{2\delta v_j^3} + \frac{3v_j\delta v_j}{2\delta v_j^3}\frac{\sin\theta_{k+1/2}J_{k+1/2j}^\theta - \sin\theta_{k-1/2}J_{k-1/2j}^\theta}{\delta\mu_k} \tag{32}$$

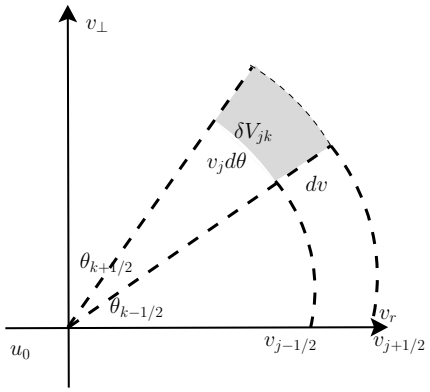

Figure 3: The suprathermal velocity grid.

where discrete elementary volumes are defined by:

$$\delta v_j^3 = v_{j+\frac{1}{2}}^3 - v_{j-\frac{1}{2}}^3, \quad \delta v_j = v_{j+\frac{1}{2}} - v_{j-\frac{1}{2}}, \quad \delta\mu_k = \cos\theta_{k+\frac{1}{2}} - \cos\theta_{k-\frac{1}{2}}.$$

The centered radial velocity v_j that appears in Eq. (32) is defined as $v_j = (v_{j+\frac{1}{2}} + v_{j-\frac{1}{2}})/2$. In those notations, the discrete volume of the cell δV_{kj} is given by :

$$\delta V_{kj} = \int_{\delta V_{kj}} 2\pi v^2 \sin\theta \, dv \, d\theta = \frac{4\pi}{3} \delta v_j^3 \delta\mu_k.$$

Besides, a straightforward centered-difference and explicit discretization of the slowing-down current leads to:

$$J^v_{kj+1/2} = \frac{u^v_{kj+1/2}}{2}(f^n_{kj+1} + f^n_{kj}) - \frac{K^{vv}_{kj+1/2}}{\delta v_{j+1/2}}(f^n_{kj+1} - f^n_{kj}) \tag{33}$$

$$J^\theta_{k+1/2j} = \frac{K^{\theta\theta}_{k+1/2j}}{v_j \delta\theta_{k+1/2}}(f^n_{k+1j} - f^n_{kj}), \tag{34}$$

where the slowing-down coefficient u and the diffusion coefficients K are explicitly given by (31) as functions of velocity. The time varying coefficients in (31) involving thermal ions and electrons are evaluated at the previous time step $t = t_n$.

4.4. A Locally Split Explicit scheme

4.4.1. Need for an explicit approach

The slowing-down and diffusion coefficients given in Eq. (31) are thus very inhomogeneous in velocity space, being highly peaked in magnitude near the thermal component region. Besides, the diffusion term is strongly anisotropic (essentially transverse) outside of the thermal component region. In such a situation, the usual implicit schemes may involve the solution of a very large and ill-conditioned linear system that will only give an approximated solution of the non-stationary problem. In this section, we demonstrate how it is possible to take advantage of the strong inhomogeneity of the slowing down current to build an efficient and simple explicit scheme that describes the non-stationary α distribution function time evolution naturally. This approach stems from ideas that were introduced in [21].

The Von Neumann stability condition for the scheme (32) in the case of constant homogeneous slowing-down coefficient u and diffusion tensor K reads as:

$$(u\,\delta t)^2 \leq 2\mathrm{Tr}(K)\,\delta t \leq \delta v^2, \tag{35}$$

where δv is the velocity mesh size. When the slowing-down coefficient u and diffusion tensor K are inhomogeneous (which is the case for our problem), we can apply (35) *locally* in each cell δV_{jk} of the suprathermal polar velocity

grid. Besides, since the scheme (32) is bi-dimensional and parametrized in polar coordinates, (35) actually leads to two stability conditions, corresponding to the radial direction v and the angular direction θ, respectively.

Treating these directions separately, the stability condition for (32) can be written for a given cell δV_{jk} as:

- in the radial v direction:

$$\left(\frac{u_j^v \delta t}{\delta v_j}\right)^2 \leq \frac{2(K_j^{vv})\delta t}{\delta v_j^2} \leq 1 \tag{36}$$

- in the angular θ direction:

$$\frac{2(K_j^{\theta\theta})\delta t}{v_j^2 \delta\theta_k^2} \leq 1. \tag{37}$$

Note that the slowing-down coefficient u as well as the diffusion tensor K given in (31) depend only on v.

The idea is then to use the explicit scheme (32) with the stability conditions (36) and (37) applied *locally* in each cell of the suprathermal grid. Indeed, the discrete scheme (32) corresponds to the finite volume formulation of a conservation equation where the time evolution of the α distribution function defined at the mesh centers is driven by the difference between the numerical fluxes calculated at the boundaries. The fluxes depend on the value of the distribution function in the neighboring cells. If the fluxes are applied during a time step Δt which is too large with respect to the absolute values of the fields in the neighboring cells, numerical instabilities occur. The idea is then to apply fluxes during a *limited* time step $\Delta t'$, possibly smaller than the imposed time step Δt. The time interval $\Delta t'$ is chosen such that the variation of the fields in the neighboring cells remain below their initial absolute values. Fluxes and fields are updated consistently at the frequency $\frac{1}{\Delta t'}$, until the imposed time step Δt is reached.

4.4.2. Stability and positivity

These conditions impose the stability of the explicit scheme (32), but not necessarily its positivity. Indeed, we have noticed that applying the explicit scheme (32) with the stability conditions (36) and (37) may lead to the development of unphysical oscillations propagating through the suprathermal velocity space. This is especially true in the velocity region where the slowing-down coefficient u is large, which may occur for example in the suprathermal region where α-particles are created.

A possible remedy is to introduce an "adaptative de-centering" in the discretization of the radial slowing-down current. We then go back to Eq. (33) and introduce the parameters η_j such as:

$$J_{kj+1/2}^v = \frac{1}{2} u_{kj+1/2}^v \left[(1-\eta_j) f_{kj+1}^n + (1+\eta_j) f_{kj}^n\right] - \frac{K_{kj+1/2}^{vv}}{\delta v_{j+1/2}} (f_{kj+1}^n - f_{kj}^n). \tag{38}$$

The choice $\eta_j = 0$ leads to the centered scheme (33), while $\eta_j = 1$ leads to a pure upwind scheme. The decentering defined in (38) may also be seen as a perturbation of the discretized diffusion term. Indeed, Eq. 38 can be written in the following form:

$$J_{kj+1/2}^v = \frac{1}{2} u_{kj+1/2}^v (f_{kj+1}^n + f_{kj}^n) - \widetilde{K}^{vv} \frac{f_{kj+1}^n - f_{kj}^n}{\delta v_{j+1/2}}. \tag{39}$$

The stability condition (36) applied with the modified coefficient diffusion $\widetilde{K}^{vv} = K_{kj+1/2}^{vv} + \frac{1}{2} u_{kj+1/2}^v \eta_j \delta v_{j+1/2}$ instead of the original K^{vv} defined in (31) leads to the stability condition:

$$\frac{1}{2}|u_{kj+1/2}^v|^2 \delta t \leq K_{kj+1/2}^{vv} + \frac{1}{2} u_{kj+1/2}^v \eta_j \delta v_{j+1/2} \quad \text{and} \quad \frac{\delta t}{\delta v_{j+1/2}^2}\left(2K_{kj+1/2}^{vv} + u_{kj+1/2}^v \eta_j \delta v_{j+1/2}\right) \leq 1.$$

Besides the positivity condition written in the case of an initial field f_α^{ST} localized in one velocity cell leads to:

$$K_{kj+1/2}^{vv} + \frac{1}{2} u_{kj+1/2}^v \eta_j \delta v_{j+1/2} \geq 0 \quad \text{and} \quad \frac{1}{\delta v_{j+1/2}}\left(2K_{kj+1/2}^{vv} + \frac{1}{2} u_{kj+1/2}^v \eta_j \delta v_{j+1/2}\right) \geq |u_{kj+1/2}^v|.$$

The minimal value of $u_v \eta$ ensuring positivity is thus:

$$u_{kj+1/2}^v \eta_j = \max\left\{0, |u_{kj+1/2}^v| - 2K_{kj+1/2}^{vv}/\delta v_{j+1/2}\right\}. \tag{40}$$

To ensure stability as well as positivity, we calculate the radial flux with respect to (39) with η_j given by (40) in each velocity cell. Actually, this amounts to using the scheme (32) with the radial diffusion coefficient K^{vv} replaced by:

$$\widetilde{K}^{vv} = \max\{K^{vv}, |u^v|\delta v/2\} \tag{41}$$

and apply the conditions (36). Note that in (36), the condition imposed on the slowing-down coefficient $|u_v|\delta t \leq \delta v$ is automatically fulfilled as soon as the one imposed on the (modified) diffusion coefficient $\widetilde{K}^{vv}$ is satisfied.

4.5. Applying the stability condition locally

We discuss now the implementation of the algorithm, named *Locally Sub-cycled Explicit* LSE algorithm that solves the problem of collisional relaxation of α-suprathermal particles. The idea is to apply the explicit scheme (32) with the stability conditions (36) and (37) applied *locally* in each cell of the suprathermal grid.

Knowing the values of the distribution function f^n_{jk} in any cell of the suprathermal velocity at time $t = t_n$, we apply the following strategy:

First step – *Local time steps calculation*

For each cell δV_{jk} of the suprathermal velocity grid, we calculate a *local* time step Δt_{jk} such that the stability conditions in the θ and v directions (37)-(36) are fulfilled. To find Δt_{jk}, the global time step, namely Δt, is halved until the stability conditions are satisfied. The local time step Δt_{jk} is then:

$$\Delta t_{jk} = \min(\Delta t^\theta_{jk}, \Delta t^v_{jk}), \tag{42}$$

where:

$$\Delta t^\theta_{jk} = 2^{-\mathrm{nsplit}^\theta_{jk}}\Delta t, \tag{43}$$

and

$$\Delta t^v_{jk} = 2^{-\mathrm{nsplit}^v_{jk}}\Delta t, \tag{44}$$

$\mathrm{nsplit}^\theta_{jk}$ (resp. nsplit^v_{jk}) is the number of times the global time step has to be halved to fulfill the stability condition in the θ (resp. v) direction.

Second step – *Sorting the cells*

Then, the cells of the suprathermal velocity grid are sorted with respect to their local time step Δt_{jk} calculated above. This can for instance be done with an efficient algorithm (e. g., 'Heapsort' [22]), which takes $O(N \ln N)$ operations for each time step where N is the number of cells of the suprathermal velocity grid. This sorting stage then allows cells to be visited by the algorithm only when they actually need to be updated, and is thus an essential step for an computationally efficient algorithm.

Third step – *Sub-cycling*

Each cell has to be advanced in both directions v and θ over a time Δt with respect to its *local* time-step Δt_{jk}, this procedure ensuring stability. We thus have to perform a *sub-cycling* for each cell. The effective computation proceeds through a loop over the smallest local time-step. Inside the loop, the fields (evaluated at the center of the cell) and the flux (evaluated at the borders) are updated consistently with the local time step of the considered cell. More precisely, we perform the following iterations:

$$\frac{f^{p+1}_{kj} - f^p_{kj}}{\Delta t_{jk}} = \frac{3v_j\delta v_j}{2\delta v_j^3}\frac{\sin\theta_{k+1/2}J^{\theta p}_{k+1/2j} - \sin\theta_{k-1/2}J^{\theta p}_{k-1/2j}}{\delta\mu_k} + \frac{1}{v_j^2}\frac{v^2_{j+\frac{1}{2}}J^{vp}_{kj+\frac{1}{2}} - v^2_{j-1/2}J^{vp}_{kj-1/2}}{2\delta v_j^3}, \tag{45}$$

where the superscript p refers to the sub-cycled iterations. The sub-cycling starts with $f^{p=0}_{kj} = f^n_{kj}$ and ends after $p^{\max}_{jk}$ iterations where $\Delta t = p^{\max}_{jk}\Delta t_{jk}$. During the process, the flux $J^\theta_{k+1/2j}$ (resp. $J^v_{kj+1/2}$) defined in (34) (resp.(39) and (40)), are updated with a frequency corresponding to $1/\Delta t^\theta_{jk}$ (resp. $1/\Delta t^v_{jk}$).

By applying the local sub-cycling described above, we are able to treat the collisional part of the Vlasov-Fokker-Planck equation governing the suprathermal component of the α distribution function using a tractable explicit approach that does not lead to prohibitive computational time.

To illustrate the efficiency of the LSE algorithm, we present in Fig. 4 the map of $\mathrm{nsplit}^\theta_{jk}$ and nsplit^v_{jk} defined in (43) and (44) on the suprathermal velocity grid. We consider two locations corresponding to the hot spot and the dense

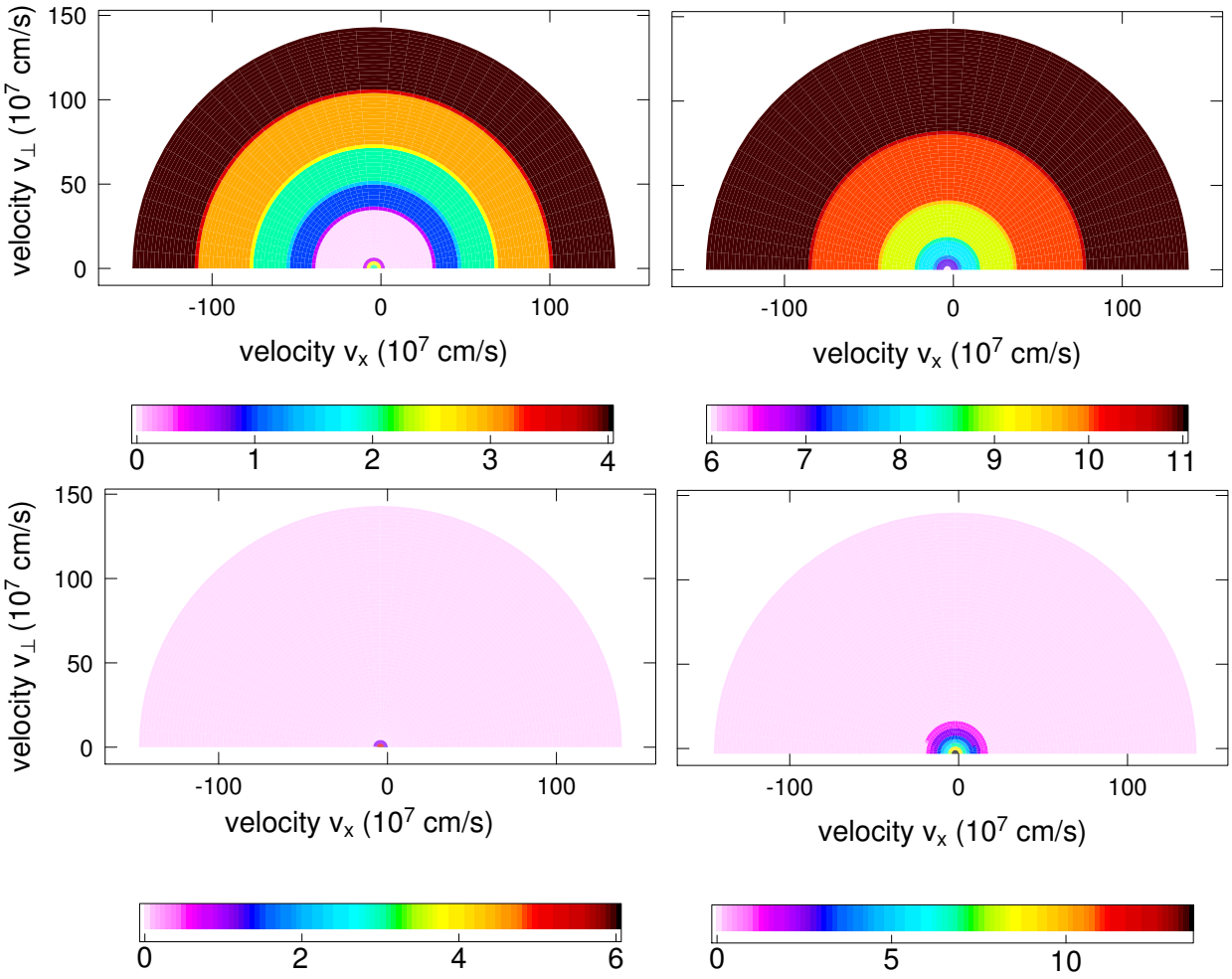

Figure 4: Map of $nsplit^v$ (top) and $nsplit^\theta$ (bottom) represented in the suprathermal velocity grid in 2 locations. On the left, we consider a point in the hot spot where: $n_e \sim 10^{21}$ cm^{-3} and $T_i \sim T_e \sim 0.5$ keV. On the right, we focus on a point taken in the dense shell where: $n_e \sim 10^{24}$ cm^{-3} and $T_i \sim T_e \sim 0.01$ keV. Those conditions correspond to a typical implosion 1 ns before stagnation. Illustrations are given for a global time step $\Delta t = 0.1$ ps

shell of a typical imploding capsule taken 1 ns before stagnation. We note that the sub-cycling is more expensive in the dense shell region than in the hot spot. Indeed, the high density and low temperature of the shell imply smaller time step.

Furthermore, considering the maps of $\text{nsplit}^\theta_{jk}$ represented at the bottom of Fig. 4, we note that to advance the fields in θ, we mainly have to sub-cycle the most central cells, where the local time step imposed by the stability condition is the smallest since the local cell size $v_j \delta\theta$ is small close to the center. For the outermost velocity cells, no sub-cycling is actually needed. More precisely, a collisional step in the dense shell taken 1 ns before stagnation, corresponding to $n_e \sim 10^{24}$ cm^{-3} (4 g.cm $^{-3}$) requires 15 subcycles. During the implosion process, the density reaches values hundred times larger, so that the explicit scheme entails smaller time steps, and more subcycles (~ 20 subcycles when $n_e \sim 10^{26}$ cm^{-3} (400 g.cm $^{-3}$)). Nevertheless, since the main part of the calculations is localized in a small central region of the suprathermal velocity space, the locally split explicit approach does not lead to prohibitive computational time (see the computational complexity analysis in Section 5.6).

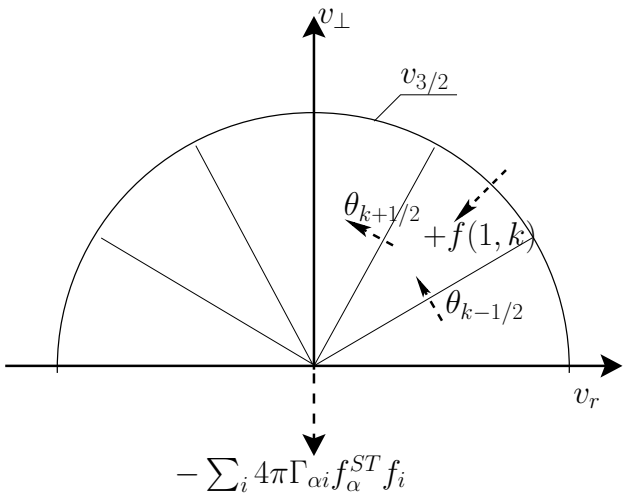

Figure 5: Central mesh of the suprathermal velocity grid

4.6. Coupling with the thermal component

We now discuss the implementation of the coupling strategy between the suprathermal and the thermal components, as described by system (18) in Section 3.2.

4.6.1. For the suprathermal component

For suprathermal α-particles, the coupling with the thermal component is made by the third term in Eq. (24) as approximated by the right-hand side of (26). It induces a time variation of the suprathermal distribution given by the following equation:

$$\left.\frac{\partial f_\alpha^{ST}}{\partial t}\right|_{ST\to T} = -\sum_i 4\pi\widetilde{\Gamma}_{\alpha i}\frac{A_\alpha}{A_i} f_\alpha^{ST} f_i \simeq -\sum_i 4\pi\widetilde{\Gamma}_{\alpha i}\frac{A_\alpha}{A_i} f_\alpha^{ST} n_i \delta^3(\vec{v}). \tag{46}$$

The time evolution of the suprathermal distribution function in central velocity meshes is then governed by:

$$\left.\frac{\partial f_\alpha^{st}}{\partial t}\right|_{\text{coll}} = \frac{1}{v^2}\frac{\partial}{\partial v}\left(v^2 J^v\right) + \frac{1}{v\sin\theta}\frac{\partial}{\partial\theta}\left(\sin\theta\, J^\theta\right) - \sum_i \widetilde{\Gamma}_{\alpha i}\frac{A_\alpha}{A_i} f_\alpha^{ST} n_i \frac{\delta(v)}{v^2}, \tag{47}$$

where the slowing-down currents J^v and J^θ are given by Eq.(28) and Eq.(29) respectively. As slowed down α-particles approach the thermal velocity region, the transverse diffusion current J^θ intensifies so that the distribution function is almost isotropic in the central velocity meshes. Eq.(47) simplifies to:

$$\left.\frac{\partial f_\alpha^{st}}{\partial t}\right|_{\text{coll}} = \frac{1}{v^2}\frac{\partial}{\partial v}\left(v^2 J^v\right) - \sum_i \widetilde{\Gamma}_{\alpha i}\frac{A_\alpha}{A_i} f_\alpha^{ST} n_i \frac{\delta(v)}{v^2}, \tag{48}$$

where the slowing-down current J_v can be approximated by:

$$J^v \simeq \widetilde{\Gamma}_{\alpha i}\frac{A_\alpha}{A_i}\frac{n_i}{v^2} f_\alpha^{ST}.$$

We then integrate Eq.(48) over a central mesh ($j = 1$, $1 \le k \le k_{\max}$) of the suprathermal velocity. The suprathermal component in the central meshes corresponding to $j = 1$ are then calculated as follows (see Fig. 5):

$$\frac{f_{k1}^{n+1} - f_{k1}^n}{\Delta t}\frac{v_{3/2}^3}{3} = \sum_i n_i \widetilde{\Gamma}_{\alpha i}(f_{k3/2}^n - f_{k1}^n). \tag{49}$$

In such a way, the distribution function remains stable in the most central part of the suprathermal velocity grid.

4.6.2. For the thermal component

To recover the full Fokker-Planck equation on the physical α distribution function $f_\alpha = f_\alpha^T + f_\alpha^{ST}$, we define an α thermal component f_α^T, which evolves on the thermal velocity grid defined above. This is also the grid on which the thermal ion D, T distribution functions evolve. This grid is actually inherited from the code Fpion, so that we use the same cylindrical parametrization as explained in [19] for the α thermal component: $f_\alpha^T(r, v_r, v_\perp)$, v_r and $v_\perp$ being the radial and tangential components of the velocity, respectively.

The term (26) subtracted from the suprathermal component equation reappears as a *source term* in the Vlasov-Fokker-Planck equation governing the thermal component of the α distribution function f_α^T, so that the relaxed suprathermal component feeds the thermal one and no α-particle is lost in the process:

$$\frac{\partial f_\alpha^T}{\partial t} + v_r \frac{\partial f_\alpha^T}{\partial r} + \frac{v_\perp}{r}\left(v_\perp \frac{\partial f_\alpha^T}{\partial v_r} - v_r \frac{\partial f_\alpha^T}{\partial v_\perp}\right) + \frac{\mathcal{E}_\alpha}{A_\alpha}\frac{\partial f_\alpha^T}{\partial v_r} = \sum_i 4\pi\widetilde{\Gamma}_{\alpha i}\frac{\partial}{\partial \vec{v}}\cdot\left(\frac{A_\alpha}{A_i} f_\alpha^T \frac{\partial \mathcal{S}_i}{\partial \vec{v}} - \nabla^2 \mathcal{T}_i \frac{\partial f_\alpha^T}{\partial \vec{v}}\right)$$
$$+\frac{1}{\widetilde{\tau}_{e\alpha}}\frac{\partial}{\partial \vec{v}}\cdot\left((\vec{v} - \vec{u_e}) f_\alpha^T + \frac{T_e}{A_\alpha}\frac{\partial}{\partial \vec{v}} f_\alpha^T\right) + \sum_i 4\pi\widetilde{\Gamma}_{\alpha i}\frac{A_\alpha}{A_i} f_\alpha^{ST} f_i. \tag{50}$$

Summing Eqs. (50) and (24) gives the original Fokker-Planck equation, so that the splitting method presented here preserves each moment associated to the α distribution function. The source term coming from the slowing down of the suprathermal component appears in the last term on the right-hand side of (50). For the thermal component, the suprathermal component f_α^{ST} appears relatively constant over the whole thermal velocity grid since it varies significantly on the coarse suprathermal velocity grid whose mesh size is of the order of the thermal velocity. That is why we use the following estimate:

$$\sum_i 4\pi\widetilde{\Gamma}_{\alpha i}\frac{A_\alpha}{A_i} f_\alpha^{ST} f_i \sim f_\alpha^{ST}(V_0)\sum_i 4\pi\widetilde{\Gamma}_{\alpha i}\frac{A_\alpha}{A_i} f_i, \tag{51}$$

V_0 being the mean ion velocity. This procedures guarantees exact mass conservation: the number of particles that are removed form the suprathermal component are injected into the thermal component. Note that the source term feeding the α thermal component depends on the thermal distribution functions of *all* thermal ion species. To solve (50), we use algorithms inherited from the code Fpion. Their numerical implementation are for example discussed in [19].

4.7. Transport and acceleration of the suprathermal component

We discuss in this section the algorithm developed to solve the Vlasov part of Eq. (24)), namely:

$$\frac{\partial f_\alpha^{ST}}{\partial t} + \vec{v}\cdot\vec{\nabla}_r f_\alpha^{ST} + \frac{\vec{\mathcal{E}}_\alpha}{A_\alpha}\cdot\frac{\partial}{\partial \vec{v}} f_\alpha^{ST} = 0 \tag{52}$$

We deal with the advection and acceleration separately.

4.7.1. Advection

In this stage, we solve the pure advection equation on the suprathermal component f_α^{ST} for a given velocity $\vec{v}$:

$$\frac{\partial f_\alpha^{ST}}{\partial t} + \vec{v}\cdot\vec{\nabla}_r f_\alpha^{ST} = 0, \tag{53}$$

whose exact solution is given by:

$$f_\alpha^{ST}(\vec{r}, \vec{v}, t + \Delta t) = f_\alpha^{ST}(\vec{r} - \vec{v}\Delta t, \vec{v}, t). \tag{54}$$

Thus, solving (53) amounts to interpolating (54) on the whole phase space. We thus start with a given point (r, v, θ) of the phase space, v, θ being chosen on the polar suprathermal velocity grid. We have to compute the transformation of the suprathermal phase space coordinates r, v, θ during one time step Δt. Since the suprathermal velocity grid is centered on the mean bulk velocity V_0, we firstly project the polar velocity coordinates on the cylindrical basis:

$$v_r = V_0 + v\cos\theta, \qquad v_\perp = v\sin\theta. \tag{55}$$

Then, we apply the following transformations on $r, v_r, v_\perp$ over one time step Δt:

$$r(t-\Delta t) = \left[r(t)^2 - 2r(t)v_r(t)\Delta t + v^2\Delta t^2\right]^{1/2}, \quad v_r(t-\Delta t) = \frac{r(t)v_r(t) - v^2\Delta t}{r(t-\Delta t)}, \quad v_\perp(t-\Delta t) = \frac{r(t)v_\perp(t)}{r(t-\Delta t)}, \tag{56}$$

which gives us the advected point in phase space. For the interpolation in space, we have to find the two consecutive nodes r_{i_0} and r_{i_0+1} of the spatial mesh such that $r_{i_0} \leq r(t-\Delta t) \leq r_{i_0+1}$. Then, for each spatial node r_{i_0} (respectively r_{i_0+1}), we have to carry out an interpolation of (56) on the polar suprathermal velocity grid centered on the local mean bulk velocity $V_0(r_{i_0})$ (respectively $V_0(r_{i_0+1})$). We thus calculate:

$$v(t-\Delta t) = \left[(v_r(t-\Delta t) - V_0(r_i))^2 + v_\perp^2(t-\Delta t)\right]^{1/2}, \quad \theta(t-\Delta t) = \cos^{-1}\frac{v_r(t-\Delta t)}{v(t-\Delta t)}, \tag{57}$$

for $i = i_0$ and $i = i_0 + 1$. We then interpolate (57) on the nodes of the suprathermal velocity grid centered on $V_0(r_i)$, using a simple linear interpolation method. This gives us the advected points:

$$f_{i_0} = f_\alpha^{ST}(r_{i_0}, v(t-\Delta t), \theta(t-\Delta t), t-\Delta t), \quad f_{i_0+1} = f_\alpha^{ST}(r_{i_0+1}, v(t-\Delta t), \theta(t-\Delta t), t-\Delta t). \tag{58}$$

The final stage is a cubic interpolation with respect to space:

$$f_\alpha^{ST}(r(t-\Delta t), v(t-\Delta t), \theta(t-\Delta t), t-\Delta t) = f_{i_0} + p\delta r \left.\frac{\partial f}{\partial r}\right|_{i_0} + p^2[3\delta f - \delta r(2\left.\frac{\partial f}{\partial r}\right|_{i_0} + \left.\frac{\partial f}{\partial r}\right|_{i_0+1}] + p^3[\delta r(\left.\frac{\partial f}{\partial r}\right|_{i_0} + \left.\frac{\partial f}{\partial r}\right|_{i_0+1}) - 2\delta f]$$

with $\delta r = r_{i_0+1} - r_{i_0}$, $\quad p = \dfrac{r(t-\Delta t) - r_{i_0}}{\delta r}$, $\quad \delta f = f_{i_0+1} - f_{i_0}$. In this equation, the spatial gradient $\dfrac{\partial f}{\partial r}(r = r_{i_0})$ is evaluated by finite differences. The slopes are limited to prevent unphysical over/undershoots in the interpolation process. More precisely, calling $u = \dfrac{r - \frac{r_{i0}+r_{i0+1}}{2}}{\delta r}$, and $\phi = \dfrac{f - \frac{f_{i0}+f_{i0+1}}{2}}{\delta r}$, we calculate local constraints applied on the slopes, such that no extremum appears inside the interval $u \in [-1/2, 1/2]$, or the value ϕ_m of the extremum of ϕ remains bounded in $[-1/2, 1/2]$. This approach is indeed similar to the one discussed in [23].

4.7.2. Acceleration

The electric field effect on the α suprathermal component is modeled by:

$$\frac{\partial f_\alpha^{ST}}{\partial t} + \frac{\vec{\mathcal{E}}_\alpha}{A_\alpha}\frac{\partial f_\alpha^{ST}}{\partial \vec{v}} = 0 \tag{59}$$

where the effective electrostatic field $\vec{\mathcal{E}}_\alpha$ is defined by Eq. (25). Here again, we use a method of characteristics to solve (59) since an acceleration can be seen as an advection in velocity. The situation gets simpler here, since we only have to carry out an interpolation in velocity on the suprathermal velocity grid. The process is repeated independently in each spatial cell.

4.8. Chain of algorithms to solve the suprathermal Vlasov-Fokker-Planck problem

We conclude this section by summarizing the sequence of algorithms that have been developed to solve the whole problem of creation, transport and collisional relaxation of suprathermal α-particles, consistently with an ion-kinetic treatment of the plasma thermal bulk. In particular, we show how the algorithms related to the suprathermal components are linked with those dealing with electrons and thermal ion distribution functions. This constitutes the main loop of our kinetic code Fuse. For a global time step Δt, we apply the following splitting sequence:

Step 1 – *Electron conductivity*

We solve the conduction part of (9), which takes the form of a pure diffusion (or heat) equation during the time $\Delta t/2$.

Step 2 – *Acceleration*

We accelerate ion thermal distribution functions for species D, T, α over the time $\Delta t/2$, and at the same time we solve the convective part of (9), which enables us to improve the energy conservation between ions and electrons (see [6]). Then, we accelerate the suprathermal α component.

Step 3 – *Advection*
We carry out the advection of thermal components for every ion species D, T, α as well as the suprathermal α component over the time $\Delta t/2$.

Step 4 – *Feeding the suprathermal component*
The suprathermal α component is fed by the fusion reaction according to (6) applied over the whole time step Δt.

Step 5 – *Suprathermal collisional relaxation*
We next solve the collisional part of (24) applying the Locally Split Explicit (LSE) algorithm over the time step Δt.

Step 6 – *Feeding the thermal component*
We apply the feeding term (51) of the α thermal component by the suprathermal one over the time step Δt.

Step 7 – *Thermal collisional relaxation*
We perform the collisional relaxation of every ion thermal distribution functions (for ion species D, T, α) on thermal ions and on electrons, applying the same algorithms as in Fpion. Note that the collisional relaxation of ion distribution functions on themselves is non-linear and is solved using Crank-Nicholson iterations with an ADI scheme (see Appendix of [20]).

Step 8 – *Advection*
Step 3 is repeated for another $\Delta t/2$.

Step 9 – *Acceleration*
Step 2 is repeated for another $\Delta t/2$.

Step 10 – *Electron conduction*
Step 1 is repeated for another $\Delta t/2$.

After each modification of the ion distribution functions (thermal or suprathermal), the ion moments as well as the slowing-down and diffusion coefficients are updated consistently.

4.9. Validation of the code by test problems

In this section, we apply the algorithms developed to model the collisional relaxation and thermalization of α-particles in simplified configurations where analytical results are known.

4.9.1. Isotropic time-dependent test problem

In this first test problem, we consider the collisional relaxation of fast α-particles in a homogeneous and steady plasma made of one mean ion species $Z_i = 1, A_i = 2.5$ and electrons. The reference density is $n_i = n_e = 10^{22}$ particles/cm^3, and the temperature is 1 keV. We keep those conditions constant during the test problem calculation. Suprathermal α-particles are then injected isotropically at the energy 3.52 MeV at a steady rate S_0 (particles.cm^{-3}.s^{-1}), so that the suprathermal component remains isotropic during the slowing down process. Following our two-scale approach, the α distribution function $f_\alpha(v,t) = f_\alpha^{ST}(v,t) + f_\alpha^{T}(v_r, v_\perp, t)$ is the solution of:

$$\begin{aligned}
\partial_t f_\alpha^{ST} &= \Gamma_{\alpha i}\frac{n_i}{v^2}\partial_v f_\alpha^{ST} + \frac{1}{\tau_{\alpha e}v^2}\partial_v\left(v^3 f_\alpha^{ST}\right) - 4\pi n_i \Gamma_{\alpha i} f_\alpha^{ST}\frac{\delta(v)}{4\pi v^2} + \frac{S_0\delta(v-v_h)}{4\pi v^2},\\
\partial_t f_\alpha^{T} &= \partial_t f_\alpha^{T}\big|_{\alpha i} + \partial_t f_\alpha^{T}\big|_{\alpha e} + 4\pi\Gamma_{\alpha i} f_i f_\alpha^{ST}(0).
\end{aligned} \tag{60}$$

$\partial_t f_\alpha^T\big|_{\alpha i}$ (resp. $\partial_t f_\alpha^T\big|_{\alpha e}$) corresponds to the collisional relaxation of thermal α-particles on thermal ions (resp. electrons).

In those conditions, we have the characteristic velocity scales, expressed in cm/s:

$$v_i^{th} \sim 3.0\times 10^7 << v_c \sim 1.1\times 10^8 << v_h \sim 1.3\times 10^9 < v_e^{th} \sim 4.2\times 10^9 \tag{61}$$

For $v > v_c$ (v_c given in Eq. (10)), the slowing down of α-particles is mainly due to the Coulomb collisions with electrons. The suprathermal component $f_\alpha^{ST}(v,t)$ then tends to the stationary solution of:

$$\partial_t f_\alpha^{ST} = \frac{1}{\tau_{\alpha e}v^2}\partial_v\left(v^3 f_\alpha^{ST}\right) + \frac{S_0\delta(v-v_0)}{4\pi v^2}. \tag{62}$$

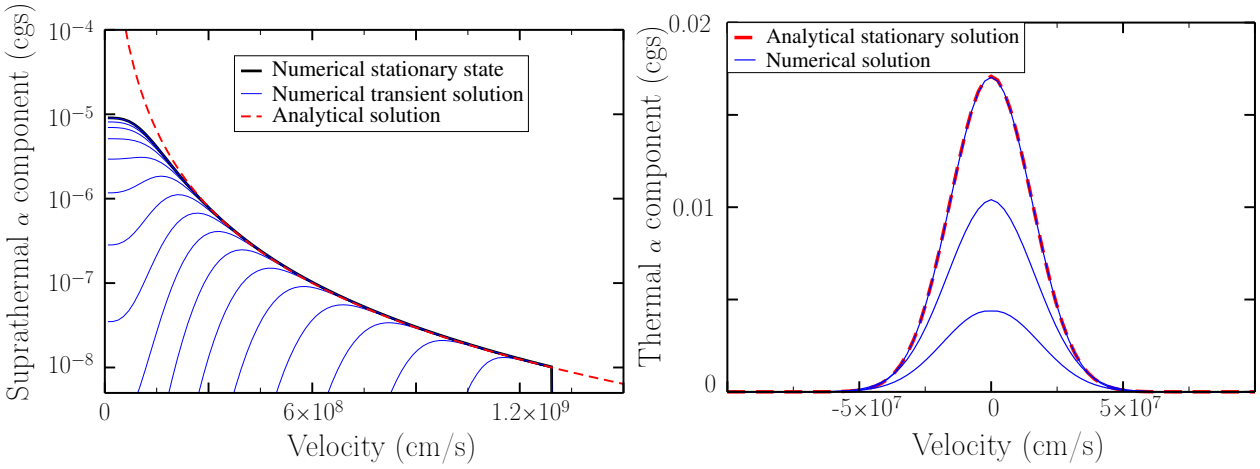

Figure 6: Time evolution of the α distribution function corresponding to the isotropic test problem. Distribution functions are expressed in cgs units, namely in $\mathrm{cm}^{-6}.\mathrm{s}^3$. The α source term is shut down after $\tau_s = 1$ ns. Left: time evolution of the α suprathermal component for $t \leq \tau_s$. The chosen time interval between 2 consecutive curves is 0.05 ns. The exact solution is represented in dashed lines. Right: time evolution of the α thermal component for $t \leq 4$ ns. The suprathermal source term is shut down after 1 ns, the α thermal component relaxes towards the Gaussian.

The stationary solution is given by [24, 25]:

$$f_1(v) = \frac{S_0 \tau_{\alpha e}}{4\pi v^3} \mathcal{H}(v_0 - v), v > v_c, \tag{63}$$

where v_h is the velocity corresponding to the injected α-particles at 3.52 MeV, which corresponds to $v_h \sim 1.3 \times 10^9$ cm/s, and $\mathcal{H}$ is the Heaviside distribution. We plot $f_\alpha^{ST}(v,t)$ calculated by Fuse at different times as well as the stationary analytical solution given by (63) (see Fig. 6). The numerical solution agrees with (63) as long as $v > v_c$. When $v < v_c$, ions tend to dominate the slowing down of α-particles and the suprathermal component solution of (60) tends to a stationary state that is almost constant close to thermal ions. This is due to the removal of the term $\propto f_\alpha^{ST} n_i \delta^3(\vec{v})$ in the collision term governing the slowing down of f_α^{ST}. The suprathermal component actually feeds the thermal one, the feeding process being driven by the source term $\propto f_\alpha^{ST}(v = 0) f_i$. The thermal component subsequently evolves towards a Maxwellian characterized by the total density n_α of α-particles injected in the system, and the reference temperature T_0 (which is kept constant during the test problem calculation):

$$\mathcal{M}_\alpha(v) = n_\alpha \left(\frac{m_\alpha}{2\pi T_0}\right)^{3/2} \exp - \frac{m_\alpha v^2}{2T_0}. \tag{64}$$

The total density of α-particles is given by:

$$n_\alpha = \int_0^{\tau_s} S_0 dt, \tag{65}$$

τ_s being the time when the source is switched off. The convergence to the Gaussian (64) is represented in Fig. 6. Note that this convergence is calculated on the refined thermal grid. The α thermal component is fed by a source term $\propto f_i$, of width $\sim \sqrt{T_0/m_i}$, and relaxes on the thermal grid towards the Gaussian (64) of width $\sim \sqrt{T_0/m_\alpha}$.

4.9.2. Anisotropic time-dependent test problem

We next consider the following anisotropic test problem. We consider an initial condition for the α suprathermal component highly localized in velocity space. Namely, we take:

$$f_\alpha^{ST}(v, \theta, t = 0) = n_\alpha \frac{\delta(v - v_0)}{4\pi v^2} \delta(\cos\theta - \cos\theta_0), \tag{66}$$

with $v_0 = v_h = 1.3 \times 10^9$cm/s and $\theta_0 = \pi/4$. We then let the suprathermal α distribution slow down on electrons and on thermal ions. As previously, the thermal plasma is homogeneous and made of one ion species $Z_i = 1, A_i = 2.5$ and electrons. The temperature of the thermal plasma is kept constant during the calculation: we take $T_0 = 5$ keV. In those conditions, the characteristic velocity scales are (in cm/s):

$$v_{th,i} \sim 6.9 \times 10^7 << v_c \sim 2.4 \times 10^8 << v_h \sim 1.3 \times 10^9 < v_{th,e} \sim 9.4 \times 10^9 \tag{67}$$

The evolution of the α distribution function is represented in Fig. 7. As long as $v > v_c$, the momentum and energy losses by the fast ions to the background plasma electrons are the dominant process. The distribution function remains highly localized in velocity space around a velocity $v_b(t)$ that declines due to the slowing down on electrons. The velocity of the bulk $v_b(t)$ can be calculated analytically [25]:

$$v_b(t) = [(v_0^3 + v_c^3) \exp -\frac{3t}{\tau_{\alpha e}} - v_c^3]^{1/3} \tag{68}$$

The comparison between the code and the exact solution is represented in Fig. 8 and reveals a good agreement, as long as $v > v_c$. Then, as $v \leq v_c$, the energy diffusion process as well as the perpendicular diffusion due to the thermal ions become significant. The α distribution function is scattered in the θ direction, due to the diffusion on the thermal ions, that intensifies as $v \to 0$. Consequently, as $v \to 0$, the α suprathermal distribution tends to become isotropic while feeding the thermal component. Finally, the thermal component converges towards the Gaussian, as in the first test problem. To properly model the vicinity of the thermalization, for $v \sim v_i^{th}$, we solve the full Coulomb operator applied to the α thermal component f_α^T that evolves on the thermal refined grid. This guarantees a proper modeling of the thermalization of the α distribution function, as it slows down, scatters and diffuses in energy in joining up with the background thermal ions.

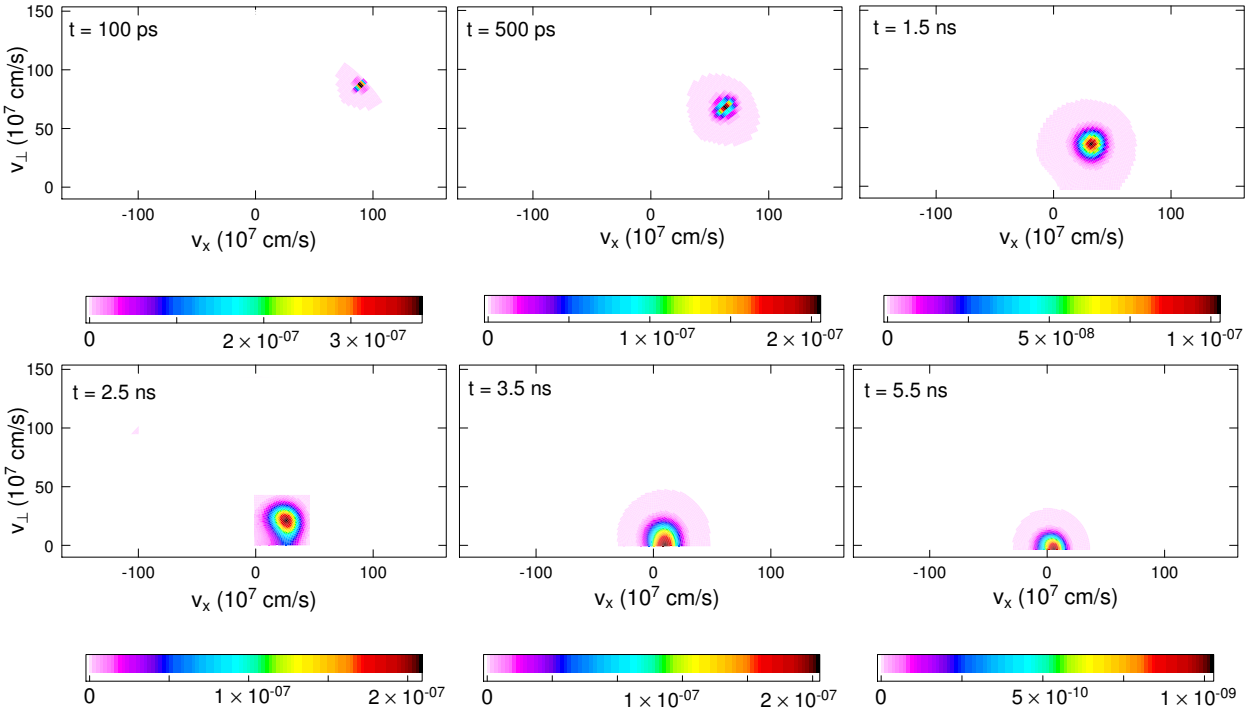

Figure 7: α suprathermal distribution solution of the anisotropic test problem at different times. Final stages of collisional relaxation. The values of the distribution function are expressed in cgs units.

4.9.3. Energy conservation and energy deposition

Although the discretized model written in the conservative form (32) ensures mass conservation, it does not rigorously conserve energy. To overcome the difficulty associated to the design of a discretized energy conservative form

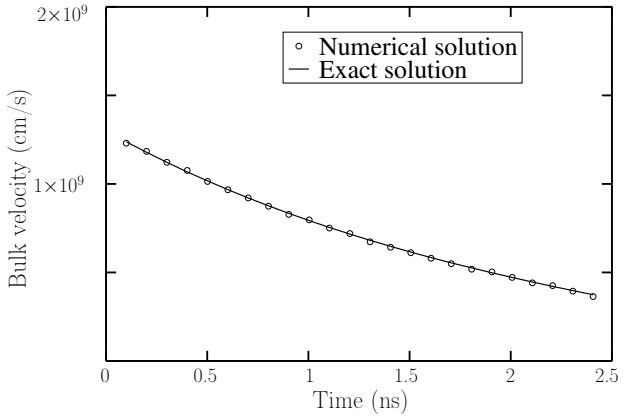

Figure 8: Time evolution of the velocity corresponding to the maximum of the α suprathermal distribution function solution corresponding to the anisotropic test problem.

of the Fokker-Planck operator, we use the following scheme: the ion energy variation $\Delta(\sum_i W_i)$ after a collision step is transfered to the electron energy, so that the total energy $\sum_i W_i + W_e$ remains constant. To control this approximation, we consider two collisonal relaxation test problems, starting from an isotropic α suprathermal component that slows down through collisions on electrons and thermal ions:

- In the first test problem, referred to "Relax 1" in Fig. 9(left), we consider the full ion/electron collisional relaxation. More precisely, at the beginning of the α relaxation process, suprathermal particles slow down essentially on electrons, as long as $v > v_c$. The electron temperature thus increases. Then, due to the collisional relaxation of thermal ions on electrons, the thermal ion temperature increases. When the suprathermal particles reach the thermal velocity region, the α thermal component builds up and the collisional relaxation between electrons and thermal ions (including the α thermal component) brings the system to a stationary state given in Fig. 9(left). The aim of this test problem is to illustrate that the way we solve the coupling between the suprathermal component and the thermal background ensures the conservation of mass, total energy and leads to a physically sound stationary state. We check that the total mass remains constant (with a numerical error less than 1% due to the finite size of the velocity mesh). We plot the time evolution of the temperatures (electrons, thermal background ions and α-thermal component) and the α-particle density (suprathermal and thermal components) in Fig. 9(left). The total energy variation of the system between the initial state and the final stationary state is less than 1%.

- In the second test problem, named "Relax 2" and represented in Fig. 9(right), the collisional relaxation between electrons and thermal ions is purposely not taken into account. As α-suprathermal particles slow down, electrons and thermal ions are heated, but collisions between electrons and thermal ions are ignored so that the electron temperature remains above the thermal ion temperature (see the time evolution of electron/thermal ion temperatures, starting from the initial state $T_e = T_i = 20$ keV in Fig. 9(right,top panel)) . This enables us to calculate accurately the fraction of α-suprathermal energy that is deposited to electrons (resp. thermal ions) during the complete slowing down of α-particles. This test case is reproduced for different initial electron temperatures. We can then compare the fraction of α-energy deposited to electrons $f_e(T_e)$ calculated by Fuse with the well-known theoretical estimate [3] $f_e(T_e) \sim \dfrac{32}{32 + T_e(\text{keV})}$, also consistent with the fluid code FCI1. Results are presented in table 2. One thus finds a good agreement between Fuse and FCI1, for this particular relaxation test problem.

.

Our original algorithm based on a two-scale approach to model the collisional relaxation between suprathermal particles and the thermal background is thus validated in simplified test problems where exact results are known.

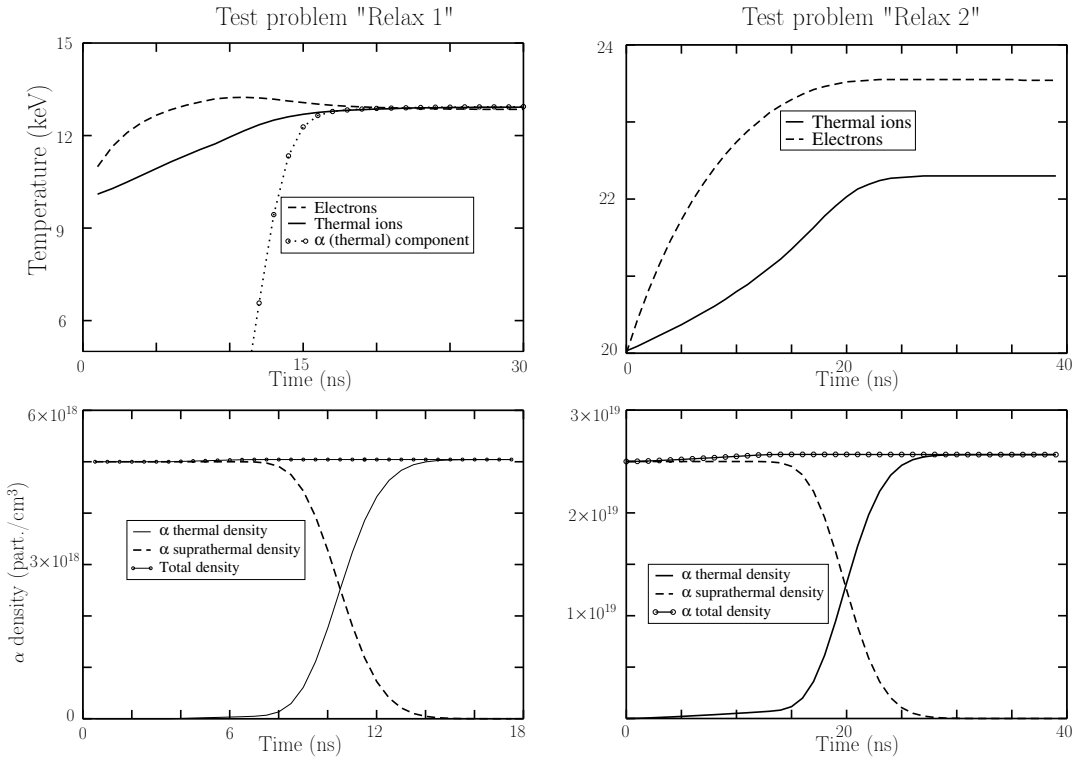

Figure 9: Time evolution of electron and thermal ion temperatures (top), as well as α density (bottom) in 2 relaxation test problems. In "Relax 1" (left), the electron/thermal ion collisional relaxation is considered so that the stationary state corresponds to a complete thermalization. In "Relax 2" (right), the electron/thermal ion collisions are disregarded on purpose. Electrons and thermal ions are exclusively heated due to the slowing down of suprathermal α-particles. In both cases, the electron density is fixed at $n_0 = 10^{22}\text{cm}^{-3}$.

Table 2: Fraction of energy deposited to electrons on the "Relax 2" test problem for different initial electron temperatures.

T_e(keV)	$f_e(T_e)$-Fluid (FCI1)	$f_e(T_e)$-Kinetic (Fuse)
5	0.86	0.81
10	0.76	0.73
15	0.68	0.65
20	0.61	0.63
50	0.39	0.40

Besides, the mass and energy conservation principles are fulfilled at a discrete level. The α energy deposition to electrons and thermal ions is also consistent with the fluid estimates. We can consider that our code Fuse is reliable. We then apply it on real target configurations.

5. Application on the ignition and thermonuclear burn of typical ICF capsules

We apply the numerical scheme presented in Section 4 to model a typical spherical implosion of a cryogenic DT capsule. Our code allows us to study ion-kinetic effects during the ignition stage and the beginning of the thermonuclear burn stage.

5.1. Initial conditions

We consider a reference fluid simulation corresponding to an ICF target with parameters typical of ignition capsules designed for NIF and LMJ laser [27, 26]. Namely, we consider a 0.3 mg cryogenic DT layer deposited on the inner surface of a CH shell of a 1 mm (inner) radius. The kinetic calculation is started at $t = 17.34$ ns after the beginning of the implosion, when the main converging shock reaches the center of the target. The boundary condition is taken from the hydrodynamic simulation. The densities, temperatures and velocities are recorded on the fuel/pusher interface in the fluid simulation.

The kinetic simulation considers three ion species, namely D, T and α. Initially, only thermal species D and T are present. They give birth to suprathermal α particles by fusion reactions. The relaxation of the suprathermal α component then leads to the creation of an α thermal component interacting with the other thermal ion distribution functions (D and T, respectively). Note that the thermal bulk is described in more detail than in [6] where a single mean ion species with a mass number of 2.5 was considered.

In our kinetic simulation, the position of each spatial meshes is updated after each time step with respect to the imposed boundary condition and to the fixed number of spatial meshes $i_{\max}$. This updating is performed before each advection phase. This means that the position of a given spatial cell r_{i_0}, with $1 \leq i_0 \leq i_{\max}$ is time dependent, decreasing with the size of the imploding system. To represent in a satisfactory manner both the dense region where the fluid simulation grid is the finest and the central zone where it is rather coarse, we employ 78 cells with a geometrically varying mesh size (with the ratio 0.97) so that the mesh size δr is decreasing from 20 μm near the center to less than one micron near the outer boundary. The thermal velocity space $(v_r, v_\perp)$ is discretized into 129×64 cells, whereas the suprathermal velocity grid (v, θ) makes use of 100×60 cells. The reference time-step value is 0.05 ps.

5.2. Comparison with Fpion and FCI1

To validate the methods related to the ion thermal components implemented in Fuse, we compare the density, velocity and temperature profiles with the hydrodynamic code FCI1 as well as with the former kinetic code Fpion at two different times of the implosion:

- at $t = 17.65$ ns, that is to say 310 ps after the beginning of implosion, we find a good agreement between the Fuse kinetic calculation and the FCI1 fluid simulation (see Fig. 10). The corresponding Coulomb logarithms spatial profiles are represented in Fig. 11 at the same observation time $t = 17.65$ ns. It can be seen that the condition $\mathrm{Log}\Lambda >> 1$ is reasonably fulfilled in the hot spot region, but not in the dense fuel shell, where the plasma is degenerated and coupled. Here, Coulomb logarithms tend to become negative. Failing anything better, we impose an artificial lower bound $\mathrm{Log}\Lambda > 1$, as discussed for instance in [28]. Degeneracy effects have nonetheless been taken into account self-consistently in the α-electron collision time, electron conductivity and electron EOS [29, 30]. We are aware that this rather crude treatment of non-ideal plasma effects may not be satisfactory, but we have tried to extend in an simple way our kinetic modeling to the dense region. Improving the kinetic modeling in the dense and coupled plasma region is a very general problem [31] that goes beyond the scope of the present study, and is left for future work.

- At $t = 18.12$ ns, in the vicinity of the target stagnation, the results of Fuse and FCI1 are still in relatively good agreement. However, we note that the compression zone near the inner interface of the dense fuel lies closer to the target center in the kinetic calculation (see the negative velocity gradient region about r = 70 μm in the right part of Fig. 12). This result has already been obtained with Fpion and discussed in [6]. This is related to a higher ion heat flux, which tends to increase the rate of ablation of the cold fuel by the hot spot. Besides, the central hot spot temperature tends to rise more quickly in the kinetic modeling. This apparent loss of synchronism between both simulations that tends to build up during the end of the implosion process is related to the way ion shock fronts are modeled. Indeed, it is known [4, 5] that ion-kinetic effects affect the structure of the shock wave propagating through the capsule, thus influencing the width of the front and the shock reflection from the hot spot center. More precisely, the kinetic shock width can be estimated by [4] $\sim (m_i/m_e)^{1/2}\lambda_{ii}$. This kinetic shock width may significantly differ from the fluid simulation where the ion front may be artificially more localized due to numerical pseudo-viscosity effects. The central temperature variations induced by the arrival of the shock waves tends to take place sooner in the kinetic simulation and in a significantly wider region than the shock width of the fluid model. Thus, starting from the same initial state, corresponding to 1 ns before

ignition, the fluid and kinetic calculations progressively loose synchronism in such a way that the hot spot ion temperature rises faster in the kinetic modeling.

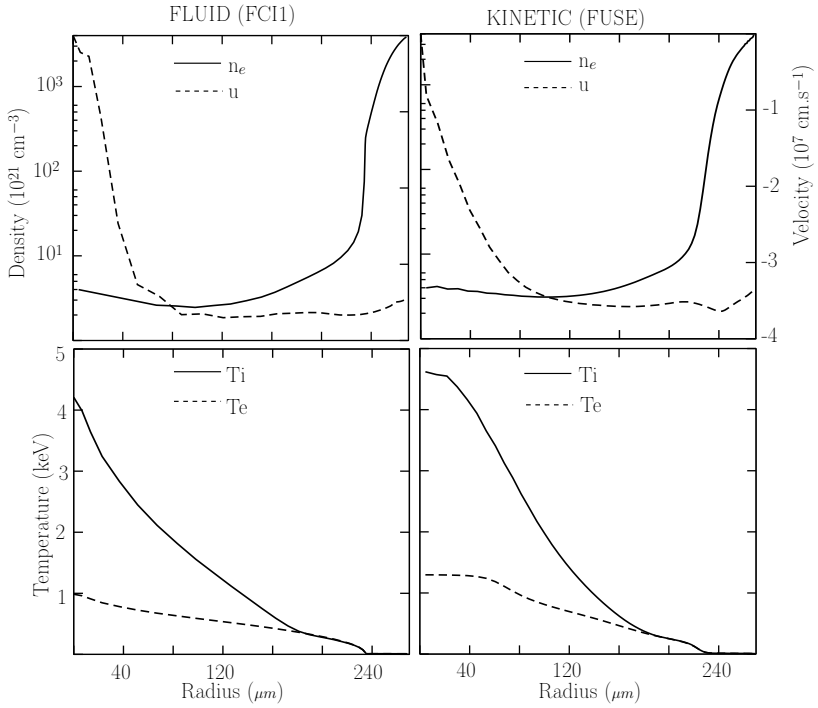

Figure 10: Comparison of the fluid(FCI1) and kinetic(FUSE) calculations. Profiles of the density, velocity and of the electron and total ion temperatures in a DT ignition target at the time t = 17.65 ns, which corresponds to 310 ps after the beginning of the kinetic calculation and roughly 650 ps before the target ignition.

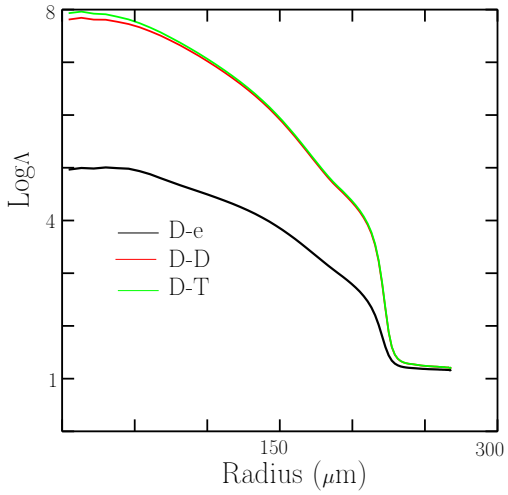

Figure 11: Coulomb logarithm spatial profiles at time t = 17650 ps.

5.3. Transport of α-particles

We analyze the transport of suprathermal α-particles throughout the capsule. Fig. 13 shows the spatial density profiles during the implosion for the suprathermal and thermal components of α-particles. At early times, suprathermal

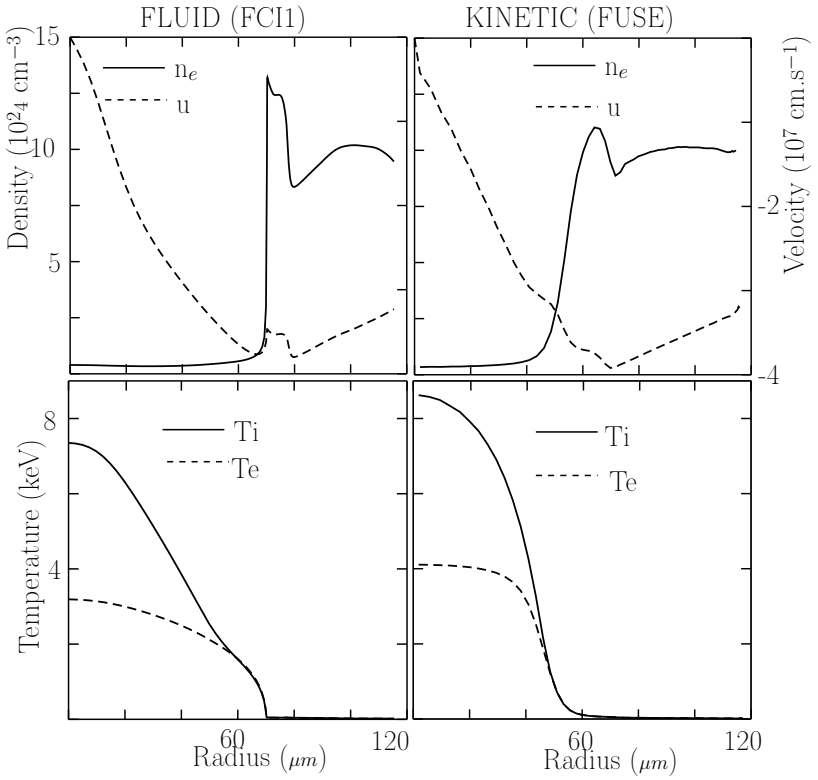

Figure 12: Comparison of the fluid(FCI1) and kinetic(Fuse) calculations. Profiles of the density, velocity and of the electron and total ion temperatures in a DT ignition target at the time t = 18.12 ns, which corresponds to 780 ps after the beginning of the kinetic calculation. This is close to the time of the target stagnation and near the beginning of ignition.

α-particles are produced in the hot central region of the capsule and deposit their energy in the surrounding cold shell. The region corresponding to the suprathermal α energy deposition is indicated by a sharp decreasing of the suprathermal density profile. This occurs at a distance which corresponds to the collisional mean free path of suprathermal α particles $\lambda_\alpha \sim 30\,\mu$m, calculated in the hot spot conditions. Meanwhile, the slowing down of suprathermal α particles feeds the thermal component, that process corresponding to the bump observed in the thermal α density profiles (Fig. 13-right).

During the implosion process, the α collisional mean free path decreases, so that the suprathermal α-particles are trapped in a smaller radius. In the mean time, the production of suprathermal α-particles intensifies due to the increasing ion temperature. As a result, the suprathermal α density increases.

It is instructive to compare the birth of the combustion wave in FCI1 and Fuse simulations. We plot in Fig. 14 the fusion reaction rate spatial profiles $\mathcal{R}_{DT}(r)$, defined in Section 2.1, for both codes. We consider three particular observation times taken just before the beginning of the combustion process. The chosen times are such that the maximum level of the reaction rate (reached in the hot spot) is of the same order of magnitude for both simulations. Fig. 14 reveals that the α-particles tend to be more localized in the hot spot in the FCI1 calculation, where a multigroup diffusion model [8] is applied. As recalled in the introduction of this article, the diffusion approximation does not hold for suprathermal α-particles in the hot spot, where the α mean free path is comparable with the hot spot radius. Applying the diffusion model tends to artificially localize the energy deposition zone inside the hot spot. Conversely, the kinetic modeling tends to enhance the transport of α-particles *out of the central hot spot*, towards the inner surface of the dense fuel shell where they eventually transfer their energy to ions and electrons. This effect may have significant consequences on the hydrodynamic profiles during the combustion phase.

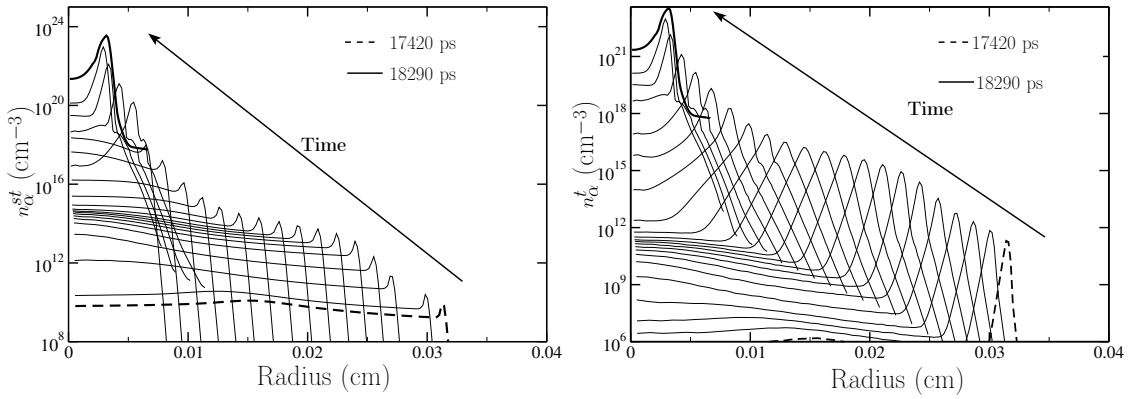

Figure 13: Density profiles of suprathermal (left) and thermal (right) α-particles. The initial time (i) corresponds to t = 17.42 ns and the final time (f) to 18.29 ns. The time interval between two consecutive profiles is 36.67 ps.

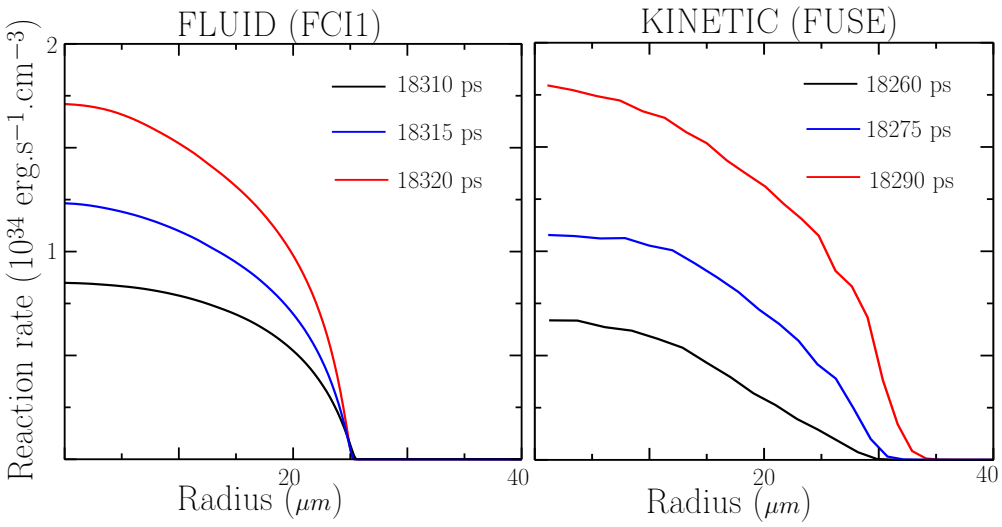

Figure 14: Comparison of the fluid and kinetic reaction rate spatial profiles just before the beginning of the combustion process.

5.4. Collisional relaxation of suprathermal α-particles

5.4.1. Anisotropy in the suprathermal region

In this section, we focus on the collisional relaxation of the suprathermal α component. We consider a given spatial cell i_0 chosen in the hot spot. The radius of the considered cell $r_{i_0}(t)$ is represented as a function of time in Fig. 15. The suprathermal distribution function of α-particles $f_\alpha^{ST}(r_{i_0}(t), v, \theta, t)$ is given in Fig. 16.

The suprathermal distribution function is rather anisotropic. It is highly peaked toward positive velocities $v_r > 0$. This can be explained by the inhomogeneous fusion reaction source term, which strongly depends on the ion local temperature. Since T_i is more peaked towards the center of the capsule, as it can be seen in the temperature profiles in Fig. 10, an observer located outside of the highly emissive central region sees the suprathermal α-particles passing from the center to the outside. This leads to a local distribution shape shown in the top panel of Fig. 16. The spatial gradient of the fusion reaction source term (6) thus accounts for the anisotropy of the suprathermal α distribution function.

Let us consider the cell i_0 with the radius such that $r_{i_0}(t) = \lambda_\alpha(\rho(t))$, where λ_α is the collisional mean free path of a suprathermal α-particle and ρ the mean density of the capsule. As α-particles deposit their energy in the considered spatial cell i_0, which corresponds to the sequence shown in Fig. 16, the suprathermal α distribution function slows down significantly towards the thermal velocity region. During this slowing down process, the distribution function

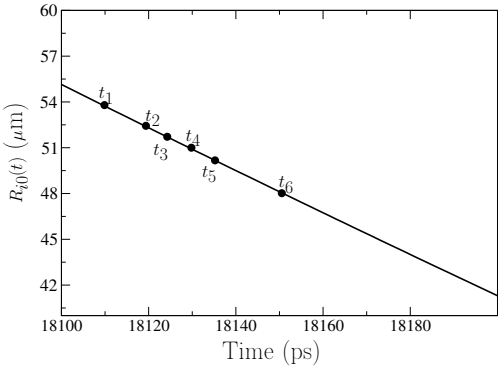

Figure 15: Time evolution of the Lagrangian radius $r_{i_0}(t)$ associated to the spatial mesh where the α-suprathermal component represented in Fig. 16 is calculated. The observation times corresponding to the sequence shown in Fig. 16 have also been indicated.

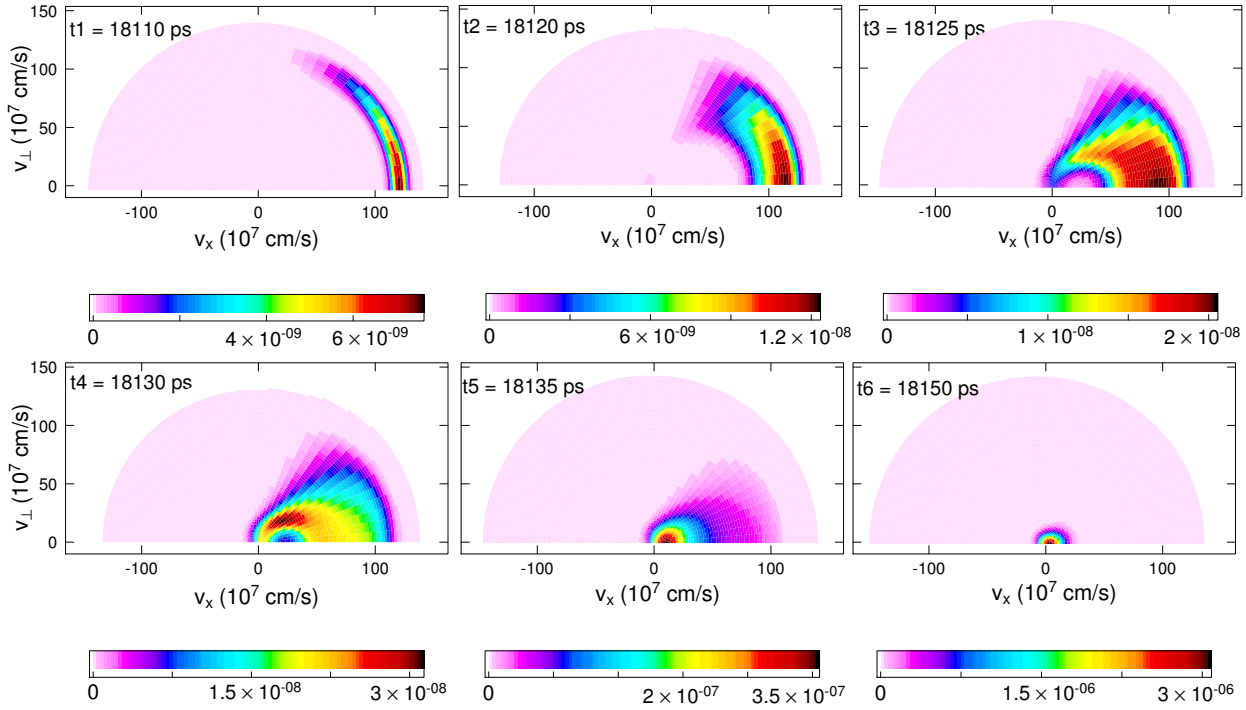

Figure 16: Distribution function of suprathermal α-particles observed in the considered hot spot mesh i_0 whose radius is represented in Fig. 15. The simulation takes into account the self-consistent modeling of creation, transport and collisional relaxation of α-particles. Times refer to beginning of the implosion and the values of the distribution function are expressed in the units presented in table 1.

tends to spread over a wider domain in the polar angle θ. This is a consequence of the diffusion part of the Fokker-Planck equation, which leads to a mainly transverse slowing-down current that intensifies close to the thermal velocity region.

To check that the collisional module of the code behaves correctly in a real target configuration, we artificially do not calculate the effect of the advection and acceleration on the α-suprathermal component, so that the time evolution is driven by the collisions on electrons and thermal ions only. The corresponding time evolution is represented in Fig. 17. This numerical test is in the same spirit as the second test problem presented in Section 4.9.2, but is carried out in thermodynamic conditions corresponding to real ICF target configuration. The suprathermal particles are initially distributed anisotropically in velocity space with respect to Fig. 17 (top-left). For $v \geq v_c \sim 3 - 4v_i^{th}$, fast ions

mostly slow down by collisional drag on the background electrons with very little pitch-angle scattering. The fast ions stay mostly in their original pitch-angle direction. For $v \leq v_c$, the suprathermal particles slow-down predominantly on the thermal background ions and scatter in pitch-angle. The suprathermal distribution function tends to be isotropic as it approaches the thermal velocity region. The suprathermal grid resolution is fine enough to represent the variations of the suprathermal component, that tends to be constant as it gets closer to the thermal velocity region.

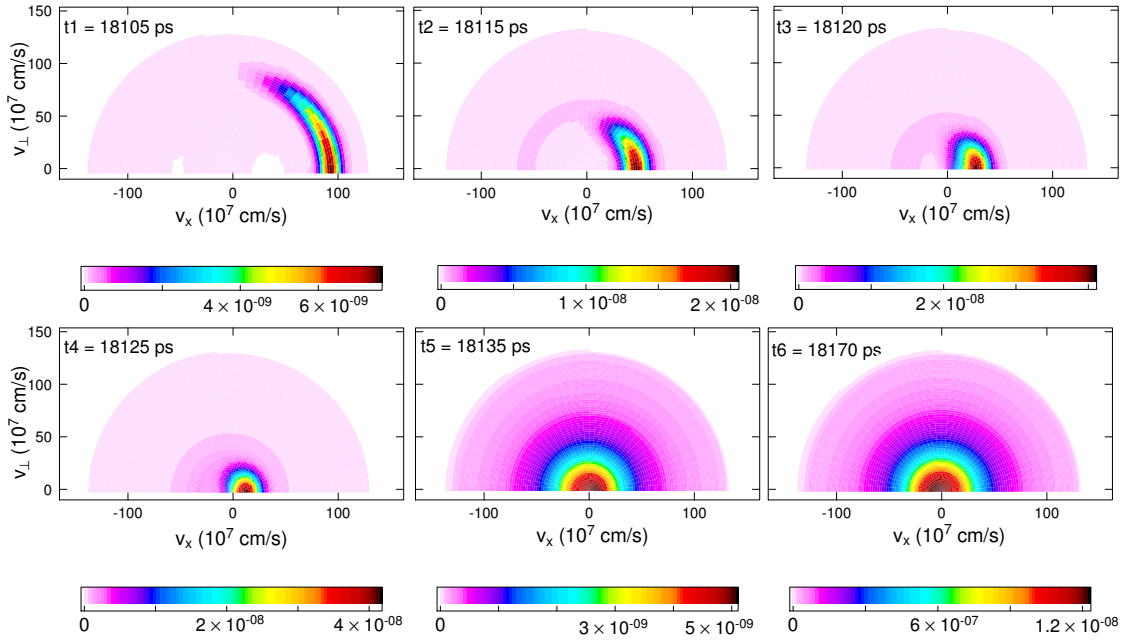

Figure 17: Distribution function of suprathermal α-particles observed in the considered hot spot mesh i_0 whose radius is represented on Fig. 15. In this sequence, the advection is purposely ignored so that the evolution of the distribution function is exclusively driven by the effects of collisions (on electrons and thermal ions). Starting from a given anisotropic initial state, the distribution function reaches an isotropic stationary state, which is peaked in the velocity region corresponding to the thermal target ions. Times refer to beginning of the implosion and the values of the distribution function are expressed in the units presented in table 1

5.4.2. Feeding the thermal component

When the slowed down suprathermal α-particles reach the thermal velocity region, a fraction of α-particles is removed from the suprathermal component, to feed the thermal component according to Eq. (50). The sequences represented in Fig. 16- 17 illustrates this coupling for the suprathermal component. The distribution function remains stable, while α-particles are accumulating in the vicinity of the thermal region. Without the removal of the term (26) on the right hand side of Eq. (24), the suprathermal distribution function would have become unstable as $v \to V_0$. The evolution of the thermal component of the α-particle distribution function represented in Fig. 18. It shows how the thermal component builds up.

5.5. Ignition and burning wave propagation

We compare the density, velocity and temperature profiles calculated during the beginning of the combustion phase by Fuse and FCI1 respectively. Results are presented in Fig. 19 and 20. The comparison is carried out until the flame arrives at the outer surface of the fuel. At latter times, the blowing off of the DT fuel is calculated self-consistently with the total pressure evaluated at the external radius of the system. The pressure tends to set in motion the remaining part of the pusher, which is not described exactly in our model but represented by a mean inertia mass, that we choose to reproduce the same dislocation as the one observed in the fluid simulation. This approximation enables us to carry out the kinetic simulation until the end of the combustion process.

In the kinetic calculation, a *pre-heating wave* tends to develop inside the dense fuel shell, while the central hot spot ion temperature remains significantly lower than in the fluid simulation. This is specially visible on the ion

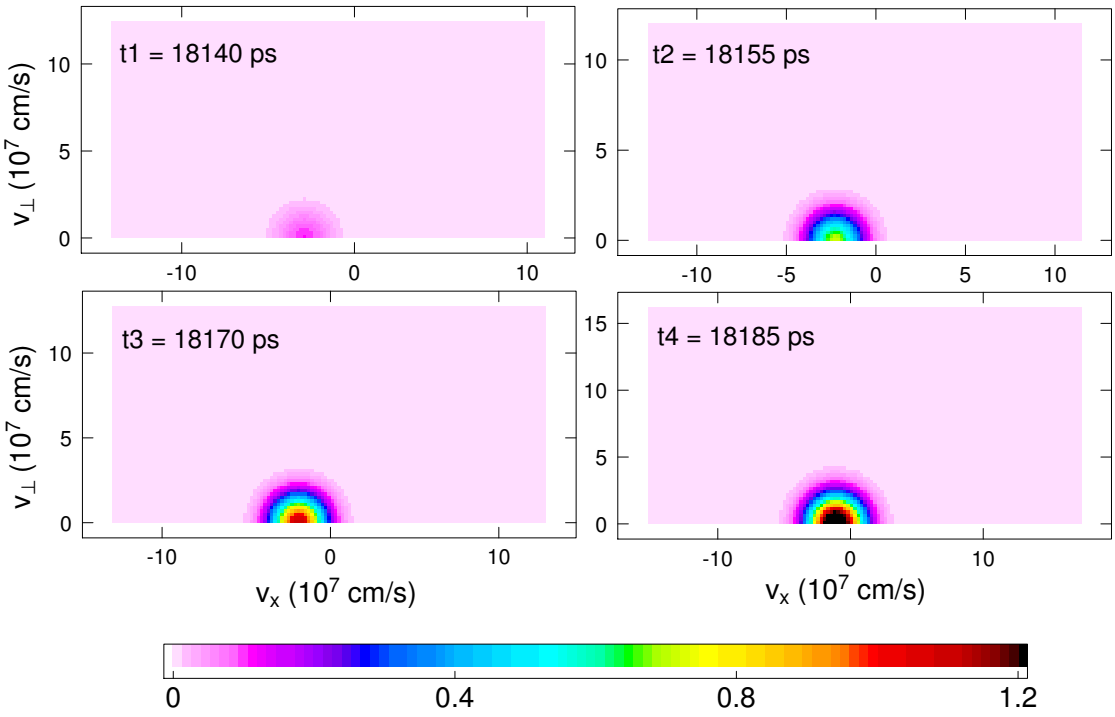

Figure 18: Thermal component of the α distribution function observed he considered hot spot mesh i_0 whose radius is represented on (Fig. 15). This thermal component is fed by the relaxation of the suprathermal component. The values of the distribution function are expressed in the units presented in table 1. Times refer to beginning of the implosion.

temperature profiles shown in Fig. 19, where a precursor builds up ahead of the main temperature front. This structure is related to the Bragg peak of the D,T ions located in the dense cold fuel. Suprathermal α-particles are created mainly in the central hot spot. Then, they deposit their energy and momentum near the inner interface of the cold fuel, where the thermal ion heating occurs. Note that the precursor is not described by the FCI1 simulation : the diffusion approximation tends to localize the α-energy deposition inside the hot spot, that reaches subsequently higher central temperatures during the combustion stage. The propagation of the burn front through the dense shell is also slower in the kinetic combustion: it takes 40 ps in the kinetic calculation, compared to 20 ps in the fluid simulation.

Besides, kinetic effects during the implosion phase are such that the heating of the hot spot happens faster. Consequently, the kinetic combustion occurs in a less dense and larger hot spot, as it is shown on the density profiles in Fig. 20,top panel. Since the regions corresponding to the suprathermal α-particle energy deposition are located farther outside the hot spot in the kinetic modeling, the dense fuel is characterized by higher mean velocities in the kinetic simulation (see Fig. 20-bottom panel).

By applying the efficient algorithm (based on a two-scale approach) exposed and validated in Section 4 on real target configurations (that could not be solved analytically), we demonstrate that the code FUSE is able to simulate real ICF targets at a kinetic level over a time corresponding to 1 ns after the start of the implosion. We are thus able to model the ignition and the beginning of the burning wave propagation. Besides, by making use of a parallelization method of the collisional part of the code (which is possible since we can calculate the effect of collisions in each spatial cell independently from the others), it takes less than 1 day of computation time, which is roughly twice as long as the usual simulations performed by FPION (corresponding to the implosion phase without α-particles).

5.6. Computational complexity analysis

It is possible to estimate the computational complexity of our two-scale kinetic approach. Let us consider a simulation time interval Δt and a global time step δt. We call N the typical size of the data structure storing the information that characterize completely the state of the system at a given time (spatial mesh, space dependent ther-

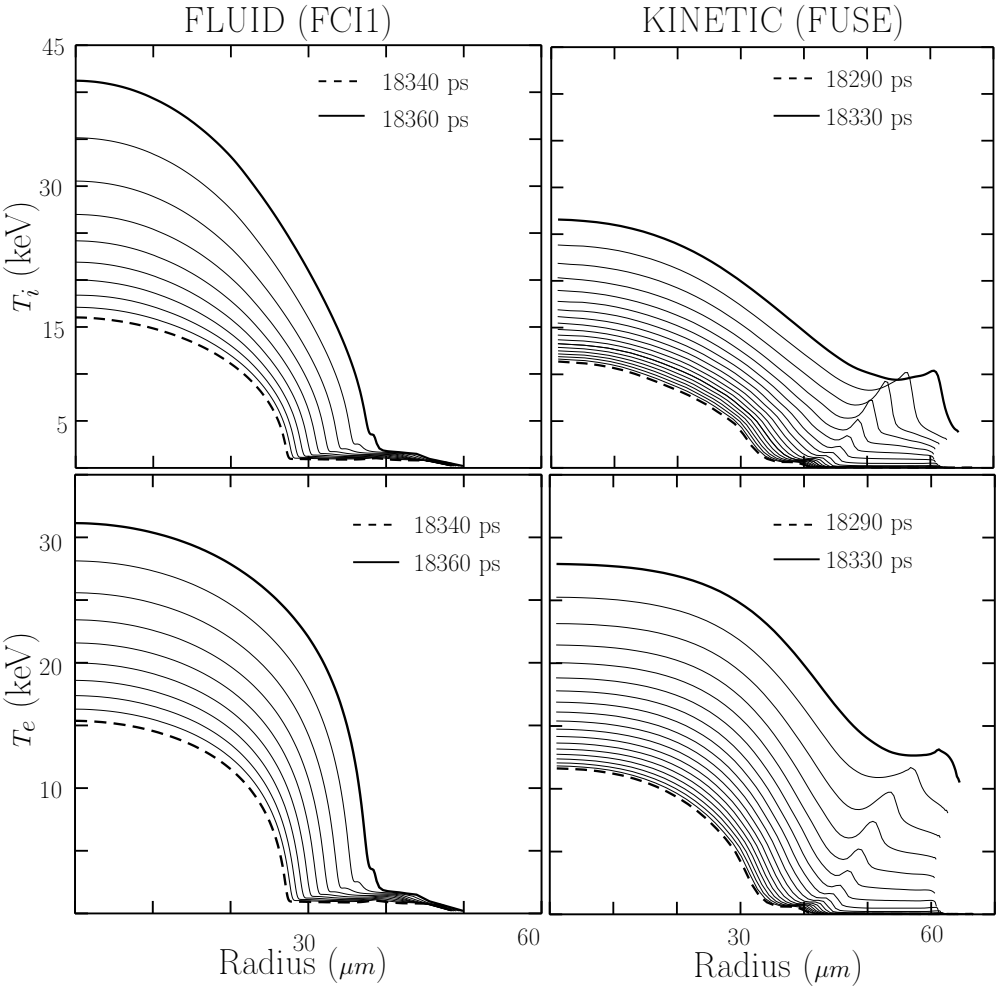

Figure 19: Comparison of the fluid(FCI1) and kinetic(Fuse) electron-ion temperatures spatial profiles during the beginning of the combustion, at times corresponding to the propagation of the flame through the dense fuel.

mal and suprathermal velocity grids, thermal distribution functions for each ion species, α suprathermal component, electron temperature spatial profile, etc). There is no CFL condition associated to the advection stage, since it is based on the characteristic methods. This is not the case for the collisional stage, where a specially-taylored explicit LSE scheme is used to advance the suprathermal component, while a standard implicit ADI approach tackles each thermal component of the considered ion species. The LSE algorithm used to model the collisional relaxation of suprathermal particles is made of two steps: a sorting of the suprathermal velocity meshes and a sub-cycling which is carried out according to a local time step δt_i calculated in each cell of the suprathermal velocity grid.

The sorting stage, based on a Heapsort algorithm takes the following number of operations :

$$\mathcal{N}_{op1} \sim O(\frac{\Delta t}{\delta t} N \mathrm{Log} N).$$

The cost of the sub-cycling can be estimated by making use of the stability condition (35) with the following order of magnitude of the diffusion tensor in a given velocity cell v_i :

$$K(v_i) \sim \frac{v_i^2}{\tau_c(v_i)} \sim \frac{v_{max}^2}{\tau_c(v_{max})} \frac{v_{max}}{v_i},$$

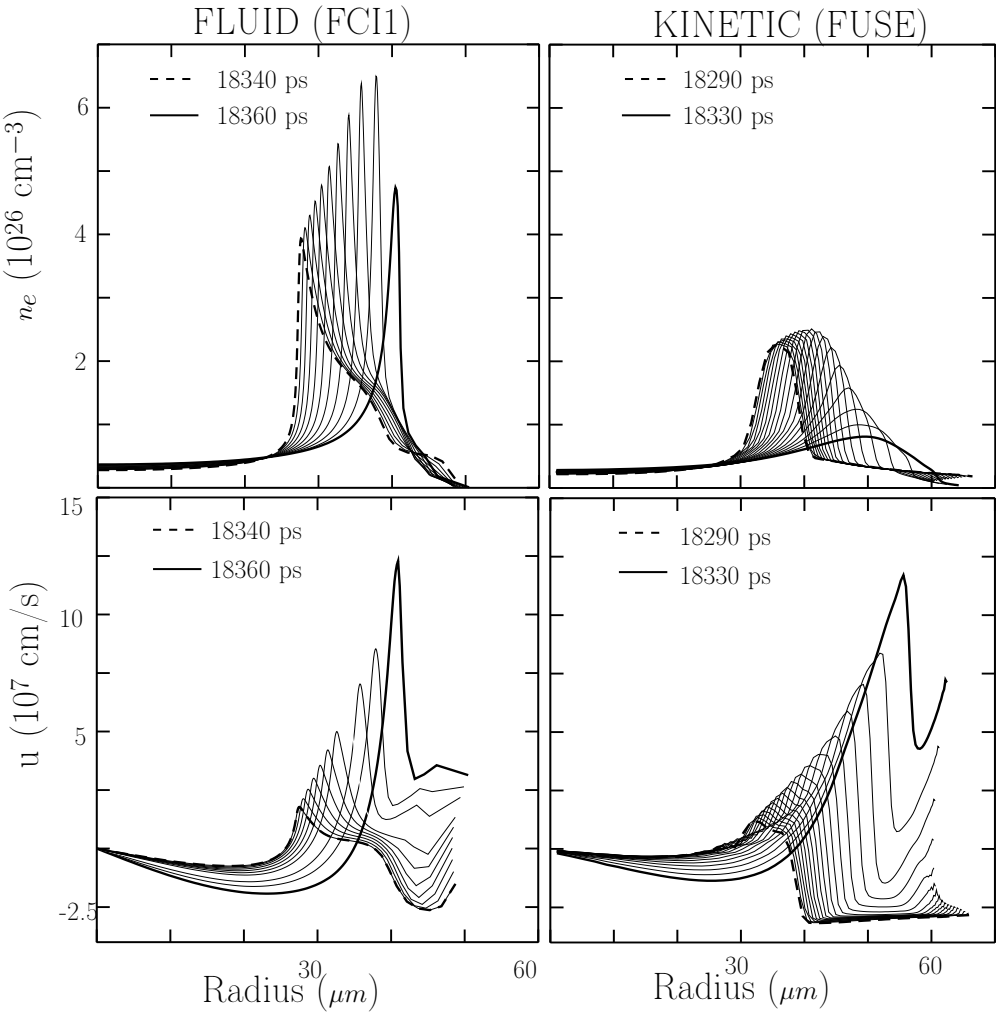

Figure 20: Comparison of the fluid(FCI1) and kinetic(FUSE) density-velocity spatial profiles during the beginning of the combustion, at times corresponding to the propagation of the flame through the dense fuel.

where v_{max} if the maximum velocity of the suprathermal mesh, and $\tau_c(v)$ the Coulomb collision time. Thus, advancing f_α^{ST} over a time Δt requires $\mathcal{N}_{op2} \sim \sum_{i=1}^{N} \frac{\Delta t}{\delta t_i}$ operations. Ref. [21] shows that $\mathcal{N}_{op2} \sim O(\frac{\Delta t}{\tau_c(v_{max})} N^2)$.

The average computational complexity of the suprathermal collisional stage is thus:

$$\mathcal{N}_{op}(\text{LSE}) \sim O(\frac{\Delta t}{\tau_c(v_{max})} N^2).$$

This is comparable with the cost of the thermal collisional stage, based on an implicit ADI scheme, which involves the inversion of a matrix of size $O(N)$ with $O(\sqrt{N})$ non vanishing diagonals. The complexity cost of this stage is then given by:

$$\mathcal{N}_{op}(\text{ADI}) \sim O(\frac{\Delta t}{\delta t} N^2).$$

This is close to $\mathcal{N}_{op}$(LSE) as long as the chosen time step is not too small compared to the typical collision time $\tau_c(v_{max})$.

In practice, one chooses $\delta t \sim 0.1$ ps, which is close to the characteristic collision time of suprathermal α-particles on electrons, in the dense shell of the DT fuel and larger than the ion-ion collision time. Such a choice allows us to

carry out a complete FUSE kinetic simulation of the implosion and burn of a typical ICF target starting 1 ns before stagnation in a reasonable computational time. A run typically takes twice as much time as a standard kinetic FPION simulation, with the same level of accuracy.

6. Summary and perspectives

We have developed a numerical strategy to model fast α-particles produced by fusion reactions at the ion kinetic level in a spherical symmetric ICF target. A two-scale approach has been specially-tailored to represent the two-component nature of the α distribution function and simulate the thermalization process accurately.

Efficient algorithms have been designed to simulate the time evolution of the fast α component, driven by the transport in the inhomogeneous thermal plasma as well as the Coulomb collisional relaxation on electrons and ions. The energy and momentum exchange between fast fusion products and the thermal plasma are thus calculated at the kinetic level. The methods have been tested in thermodynamic conditions corresponding to typical DT targets close to ignition. It has been shown that a locally split explicit scheme can be used to describe the fast α population evolution in non-prohibitive computational time. Besides, the algorithms presented here are easily parallelizable to take advantage of present-day multi-core architectures.

The ion-kinetic code FUSE, built as an extension of the former code FPION, is thus able to model a full DT target implosion, including the ignition and burn processes, at a ion-kinetic level. Investigating in more detail the role of kinetic effects of fusion products in the ignition and burn of DT targets is the purpose of ongoing work and will be published elsewhere [32]. We may have in view to study implosions in the vicinity of the ignition threshold, where kinetic effects should be enhanced and may modify the energy gain and threshold position.

Finally, the two-component formalism devised for α-particles could be naturally extended to add the effect of Boltzmann-type large angle scattering, that would feed a suprathermal component for the D-T ions. Neutron momentum and energy deposition may also be modeled in a similar way. This extension is left for future work.

Acknowledgments. The authors are grateful to Professors Xavier Blanc, Josselin Garnier, Rémi Sentis for fruitful discussions on the subject.

[1] J. D. Lindl, Inertial Confinement Fusion – The quest for ignition and energy gain using indirect drive, Springer Verlag, New York, 1998.
[2] S. Atzeni and J. Meyer-ter-Vehn, The physics of inertial fusion, Oxford, Oxford University Press, 2004.
[3] G. S. Fraley, E. J. Linnebur, R. J. Mason, R. L. Morse, Thermonuclear burn characteristics of compressed deuterium-tritium microspheres, Phys. Fluids 17 (1974) 474.
[4] M. Casanova, O. Larroche, J.-P. Matte, Kinetic study of a shock wave in a high-temperature plasma, Phys. Rev. Lett. 67 (1991) 2143.
[5] F. Vidal, J.-P. Matte, M. Casanova, O. Larroche, Spherical ion kinetic simulations of DT implosions, Phys. Rev. E 52 (1995) 4568.
[6] O. Larroche, Kinetic simulations of fuel ion transport in ICF target implosions, Eur. Phys. J. D 27 (2003) 131.
[7] P. A. Haldy, J. Ligou, A moment method for calculating the transport of energetic charged particles in hot plasmas, Nucl. Fusion 17 (1977) 6.
[8] E. G. Corman, W. E. Loewe, G. E. Cooper, A. M. Winslow, Multi-group diffusion of energetic charged particles, Nucl. Fusion 15 (1975) 377.
[9] G. C. Pomraning, Flux-limited diffusion and Fokker-Planck equations, Nucl. Sci. Eng. 85 (1983) 116.
[10] J. J. Honrubia, Nuclear fusion by inertial confinement - A comprehensive treatise, G. Velarde, Y. Ronen, J. M. Martinez-Val (CRC Press, Boca Raton, Florida, 1993), chap. 9, p. 211.
[11] B. Lapeyre, E. Pardoux, R. Sentis, Monte Carlo methods fo transport and diffusion equations, Oxford University Press, 2003.
[12] F. Chaland, R. Sentis, Two-temperature Euler equations for a plasma with slowing down of suprathermal particles, Int. Numer. Meth. Fluids 56 (2008) 1489.
[13] T. A. Mehlhorn, J. J. Duderstadt, A discrete ordinates solution of the Fokker-Planck equation characterizing charged particle transport, J. Comput. Phys. 38 (1980) 1.
[14] J. Killeen, K. D. Marx, The solution of the Fokker-Planck equation for a mirror-confined plasma, Meth. Comput. Phys. 9 (1970) 422.
[15] M. N. Rosenbluth, W. M. MacDonald, D. L. Judd, Fokker-Planck equation for an inverse-square force, Phys. Rev. 107 (1957) 1.
[16] P. Degond, B. Lucquin-Desreux, Comportement hydrodynamique d'un mélange gazeux formé de deux espèces de masse très différentes, C. R. Acad. Sci. Paris 322 (1996) 405.
[17] S. I. Braginskii, Transport Processes in a Plasma, Reviews of Plasma Physics, V. 1, M. A. Leontovich ed. Consultants Bureau, New York, 1965, p. 205.
[18] L. Spitzer, R. Härm, Transport phenomena in a completely ionized gas, Phys. Rev. 89 (1953) 977.
[19] O. Larroche, Kinetic simulation of a plasma collision experiment, Phys. Fluids B 5, 8 (1993) 2816.
[20] C. Chenais-Popovics *et al.*, Kinetic to thermal energy transfer and interpenetration in the collision of laser-produced plasmas, Phys. Plasmas 4 (1997) 190.
[21] O. Larroche, An efficient explicit numerical scheme for diffusion-type equations with a highly inhomogeneous and highly anisotropic diffusion tensor, J. Comput. Phys. 223 (2007) 436.
[22] W. H. Press, S. A. Teukolsky, W. T. Vetterling and B. P. Flannery, Numerical recipes in C, Cambridge University Press, Cambridge, 1992.
[23] F. N. Fritsch, R. E. Carlson, Monotone Piecewise Cubic Interpolation , SIAM J. Numer. Anal. 17 (1980) 238.
[24] Y.N. Dnestrovskii, D. P. Kostomaroc, Numerical simulation of plasmas, Chapter 2 p55, Springer 1985.

[25] J.M. Rax, Physique des Plasmas, Chapter 12 and references therein, Dunod, 2008.
[26] P. A. Bradley, D. C. Wilson, Two-dimensional capsule-hohlraum designs for the National Ignition Facility, Phys. Plasmas 8 (2001) 3724 and references therein.
[27] Y. Saillard, Hydrodynamique de l'implosion d'une cible FCI, C. R. Acad. Sci. Paris t. 1 sér. IV (2000) 705.
[28] Y. T. Lee, R. M. More, An electron conductivity model for dense plasmas, Phys. Fluids. Anal 27 (1984) 1273.
[29] H. Brysk, Electron-ion equilibration in a partially degenerate plasma, Plasma Physics 16 (1974) 927.
[30] H. Brysk, P. M. Campbell, P. Hammerling, Thermal conduction in laser fusion, Plasma Physics 17 (1975) 473.
[31] C. K. Li, R. D. Petrasso, Fokker-Planck equation for moderately coupled plasmas, Phys. Rev. Lett. 70 (1993) 3059.
[32] B.E Peigney, O. Larroche, V. Tikhonchuk, Ion kinetic effects on the ignition and burn of ICF targets, in preparation.